

EMPIRICAL PREDICTION OF  
NEAR-SOURCE SOIL AND SOFT-ROCK GROUND MOTION  
FOR THE DIABLO CANYON POWER PLANT SITE,  
SAN LUIS OBISPO COUNTY, CALIFORNIA

by

Kenneth W. Campbell

Prepared for

Lawrence Livermore National Laboratory

Dames & Moore

Evergreen, Colorado

September 1990

9101030295 901221  
PDR ADOCK 05000275  
R PDR



# CONTENTS

Tables.....	ii
Figures.....	iv
Introduction.....	1
Ground-Motion Model.....	1
Strong-Motion Data Base.....	3
Regression Analysis.....	4
Results for Peak Parameters.....	5
Results for Response Spectra.....	5
Significance of Results.....	8
Soft-Rock Sites.....	8
Discussion of Results.....	9
Ground-Motion Saturation.....	9
Style of Faulting.....	9
Building Effects.....	9
Source Directivity.....	10
Sediment Depth.....	10
Distribution of Residuals.....	10
Ground-Motion Estimates for Diablo Canyon.....	11
References.....	12



## TABLES

Table		Page
1	Regression coefficients: Horizontal components.....	17
2	Regression coefficients: Vertical components.....	17
3	Regression coefficients: Building effects.....	18
4	Standard errors: Horizontal components.....	18
5	Standard errors: Vertical components.....	19
6	Site-specific estimates of strong ground motion: Diablo Canyon site, California ( $M_S = 7.2$ , $R = 4.7-5.1$ km, $D = 4$ km)....	19
A-1	Earthquake data—soil sites: Peak parameters.....	34
A-2	Strong-motion data—soil sites: Peak parameters.....	35
A-3	Station data—soil sites.....	40
A-4	Earthquake data—soil sites: 0.04 sec pseudorelative velocity.....	44
A-5	Earthquake data—soil sites: 0.05 sec pseudorelative velocity.....	44
A-6	Earthquake data—soil sites: 0.075–1.0 sec pseudorelative velocity....	45
A-7	Earthquake data—soil sites: 1.5–2.0 sec pseudorelative velocity.....	46
A-8	Earthquake data—soil sites: 3.0 sec pseudorelative velocity.....	47
A-9	Earthquake data—soil sites: 4.0 sec pseudorelative velocity.....	48
A-10	Strong-motion data—soil sites: 0.04 sec pseudorelative velocity.....	49
A-11	Strong-motion data—soil sites: 0.05 sec pseudorelative velocity.....	51
A-12	Strong-motion data—soil sites: 0.075 sec pseudorelative velocity.....	54
A-13	Strong-motion data—soil sites: 0.1 sec pseudorelative velocity.....	57
A-14	Strong-motion data—soil sites: 0.15 sec pseudorelative velocity.....	60
A-15	Strong-motion data—soil sites: 0.2 sec pseudorelative velocity.....	63
A-16	Strong-motion data—soil sites: 0.3 sec pseudorelative velocity.....	66
A-17	Strong-motion data—soil sites: 0.4 sec pseudorelative velocity.....	69
A-18	Strong-motion data—soil sites: 0.5 sec pseudorelative velocity.....	72
A-19	Strong-motion data—soil sites: 0.75 sec pseudorelative velocity.....	75
A-20	Strong-motion data—soil sites: 1.0 sec pseudorelative velocity.....	78
A-21	Strong-motion data—soil sites: 1.5 sec pseudorelative velocity.....	81
A-22	Strong-motion data—soil sites: 2.0 sec pseudorelative velocity.....	84
A-23	Strong-motion data—soil sites: 3.0 sec pseudorelative velocity.....	87
A-24	Strong-motion data—soil sites: 4.0 sec pseudorelative velocity.....	90
A-25	Earthquake data—soft-rock sites: Peak parameters.....	93
A-26	Strong-motion data—soft-rock sites: Peak parameters.....	94
A-27	Station data—soft-rock sites.....	95
A-28	Earthquake data—soft-rock sites: 0.04 sec pseudorelative velocity....	96
A-29	Earthquake data—soft-rock sites: 0.05–2.0 sec pseudorelative velocity	96
A-30	Earthquake data—soft-rock sites: 3.0 sec pseudorelative velocity.....	96
A-31	Earthquake data—soft-rock sites: 4.0 sec pseudorelative velocity.....	96
A-32	Strong-motion data—soft-rock sites: 0.04 sec pseudorelative velocity.	97
A-33	Strong-motion data—soft-rock sites: 0.05 sec pseudorelative velocity.	97
A-34	Strong-motion data—soft-rock sites: 0.075 sec pseudorelative velocity	98



## TABLES

<i>Table</i>		<i>Page</i>
A-35	Strong-motion data—soft-rock sites: 0.1 sec pseudorelative velocity ..	99
A-36	Strong-motion data—soft-rock sites: 0.15 sec pseudorelative velocity .	100
A-37	Strong-motion data—soft-rock sites: 0.2 sec pseudorelative velocity ..	101
A-38	Strong-motion data—soft-rock sites: 0.3 sec pseudorelative velocity ..	102
A-39	Strong-motion data—soft-rock sites: 0.4 sec pseudorelative velocity ..	103
A-40	Strong-motion data—soft-rock sites: 0.5 sec pseudorelative velocity ..	104
A-41	Strong-motion data—soft-rock sites: 0.75 sec pseudorelative velocity .	105
A-42	Strong-motion data—soft-rock sites: 1.0 sec pseudorelative velocity ..	106
A-43	Strong-motion data—soft-rock sites: 1.5 sec pseudorelative velocity ..	107
A-44	Strong-motion data—soft-rock sites: 2.0 sec pseudorelative velocity ..	108
A-45	Strong-motion data—soft-rock sites: 3.0 sec pseudorelative velocity ..	109
A-46	Strong-motion data—soft-rock sites: 4.0 sec pseudorelative velocity ..	110



## FIGURES

<i>Figure</i>		<i>Page</i>
1	Magnitude versus distance: peak acceleration (soil) .....	20
2	Magnitude versus distance: peak acceleration (soft rock) .....	21
3	Magnitude versus distance: peak velocity (soil) .....	22
4	Magnitude versus distance: peak velocity (soft rock) .....	23
5	Attenuation relationships: peak acceleration; strike-slip faults; $M = 5.0, 6.5, 8.0$ .....	24
6	Attenuation relationships: peak velocity; strike-slip; $M = 5.0, 6.5, 8.0$ ; $D = 0$ km .....	25
7	Pseudorelative velocity spectra: 5% damped PSRV spectra; strike-slip; $M = 5.0, 6.5, 8.0$ ; $R = 10$ km; $D = 0$ km .....	26
8	Pseudorelative velocity spectra: 5% damped PSRV spectra; strike-slip; $R = 10, 25, 50$ km; $M = 6.5$ ; $D = 0$ km .....	27
9	Predicted LTSP analysis spectra: horizontal PSAA spectra; strike-slip; $M = 7.2$ ; $R = 4.9$ km; $D = 4.0$ km .....	28
10	Predicted LTSP analysis spectra: vertical PSAA spectra; strike-slip; $M = 7.2$ ; $R = 4.9$ km; $D = 4.0$ km .....	29
11	Predicted LTSP analysis spectra: horizontal PSAA spectra; reverse oblique; $M = 7.2$ ; $R = 4.7$ km; $D = 4.0$ km .....	30
12	Predicted LTSP analysis spectra: vertical PSAA spectra; reverse oblique; $M = 7.2$ ; $R = 4.7$ km; $D = 4.0$ km .....	31
13	Predicted LTSP analysis spectra: horizontal PSAA spectra; thrust; $M = 7.2$ ; $R = 5.1$ km; $D = 4.0$ km .....	32
14	Predicted LTSP analysis spectra: vertical PSAA spectra; thrust; $M = 7.2$ ; $R = 5.1$ km; $D = 4.0$ km .....	33



# EMPIRICAL PREDICTION OF NEAR-SOURCE SOIL AND SOFT-ROCK GROUND MOTION FOR THE DIABLO CANYON POWER PLANT SITE, SAN LUIS OBISPO COUNTY, CALIFORNIA

## INTRODUCTION

In 1985, Pacific Gas and Electric Company (PG&E) initiated a three-year program to reassess the seismic design basis of the Diablo Canyon power plant, San Luis Obispo County, California, as part of a licensing condition imposed by the U. S. Nuclear Regulatory Commission (NRC). The results of the program have been summarized in a PG&E report entitled *Final Report of the Diablo Canyon Long Term Seismic Program for the Diablo Canyon Power Plant* (PG&E, 1988).

During this same period, NRC commissioned the author to conduct an independent analysis of near-source ground motion for the Diablo Canyon site (Campbell, 1989a). Due to project constraints, the attenuation relationships developed during that study were restricted to soil recordings. The study concluded, however, that soil recordings and soft-rock recordings were statistically indistinguishable. As a result, the report recommended that the two data bases be combined to develop near-source attenuation relationships. The current report documents the results of this latter study.

The first part of the report describes the ground-motion model, the near-source data base, and the regression analyses used to derive the attenuation relationships developed during the course of the study. In the second part of the report, these attenuation relationships are used to provide estimates of peak acceleration, peak velocity, and five-percent damped pseudoabsolute acceleration response spectra at the Diablo Canyon site for a proposed  $M = 7.2$  earthquake on the nearby Hosgri fault.

## GROUND-MOTION MODEL

Strong-motion parameters of interest in this study are peak horizontal acceleration (PHA), peak vertical acceleration (PVA), peak horizontal velocity (PHV), peak vertical velocity (PVV), horizontal 5% damped pseudorelative velocity response spectra (PSRVH), and vertical 5% damped pseudorelative velocity response spectra (PSRVV). The response spectra are represented by 15 ordinates whose periods,  $T$ , range from 0.04 to 4.0 sec, or equivalently, whose frequencies range from 0.25 to 25 Hz. Consistent with recommendations by Campbell (1982, 1985), horizontal parameters of ground motion were computed from the arithmetic mean of the two horizontal components.



The relationship used to model the near-source attenuation of strong ground motion is given by the expression,

$$\ln Y = a + bM + d \ln [R + c_1 \exp(c_2 M)] + cF + f_1 \tanh [f_2(M + f_3)] + g_1 \tanh (g_2 D) + \sum_{i=1}^3 h_i K_i + \epsilon, \quad (1)$$

where  $Y$  is the strong-motion parameter of interest;  $M$  is earthquake magnitude [ $M_L$  for  $M < 6.0$  and  $M_S$  for  $M \geq 6.0$ , consistent with the moment-magnitude scale proposed by Hanks and Kanamori (1979)];  $R$  is distance to seismogenic rupture in kilometers (hereafter referred to as seismogenic distance);  $F$  is a parameter representing the style of faulting [ $F = 0$  for strike-slip faults,  $F = 1$  for reverse, reverse-oblique, thrust, and thrust-oblique faults (hereafter referred to as reverse faults)];  $D$  is depth to basement rock (sediment depth) in kilometers;  $K_i$  is a parameter representing building effects ( $K_1 = 1$  for embedded buildings 3-11 stories in height,  $K_2 = 1$  for embedded buildings greater than 11 stories in height,  $K_3 = 1$  for nonembedded buildings greater than 2 stories in height,  $K_1 = K_2 = K_3 = 0$  for all other recording sites);  $\epsilon$  is a random error term with a mean of zero and a standard deviation of  $\sigma$ , the standard error of regression;  $\tanh(*)$  is the hyperbolic tangent function; and  $a, b, \dots, h_i$  are regression coefficients to be determined by the data.

The nonlinear term,  $R + c_1 \exp(c_2 M)$ , is used to model magnitude-dependent attenuation of ground motion. First proposed by Esteva (1970), this term has been used successfully by many investigators to model the near-source attenuation of both observed and simulated ground motions (e.g., Campbell, 1981, 1987, 1989a; Hadley *et al.*, 1982; Sadigh, 1983; Joyner and Boore, 1988; among others). Note that when  $c_2 = -b/d$ ,  $Y$  becomes independent of magnitude (*i.e.*, it "saturates") at  $R = 0$ , the presumed source of the ground motion.

The magnitude term,  $f_1 \tanh [f_2(M + f_3)]$ , has been proposed by Campbell (1989a) to model the observed nonlinear dependence of pseudorelative velocity response (PSRV) on magnitude for  $T > 0.3$  sec; and the sediment-depth term,  $g_1 \tanh (g_2 D)$ , has been proposed by Campbell (1987) to model the observed nonlinear dependence of peak velocity and PSRV (for  $T > 0.75$  sec) on depth to basement rock. The hyperbolic tangent function was used to model these nonlinear terms because of several unique characteristics: (1) it is zero when its argument is zero, (2) it is nearly linear at relatively small values of its argument, and (3) it asymptotically approaches a value of one at relatively large values of its argument. This makes  $\tanh$  well-suited to modelling the observed magnitude and depth dependence of the ground-motion recordings.

For a given earthquake, seismogenic distance,  $R$ , is defined as the shortest distance between a recording site and the assumed zone of seismogenic rupture. Implicit in this definition is the assumption that faulting within the sediments and shallow crust is non-seismogenic—*i.e.*, it is associated with a very low dynamic stress drop—and does not



contribute significantly to recorded strong ground motion at frequencies of engineering interest. In all cases, seismogenic rupture was carefully determined from spatial distributions of aftershocks, from earthquake modelling studies, from regional crustal velocity studies, and from geodetic and geologic data.

Unlike the distance measures proposed by Campbell (1981) and Shakal and Bernreuter (1981), the above definition of distance avoids ambiguities associated with the identification and specification of surface fault rupture and fault asperities (Boore and Joyner, 1982; Campbell, 1985), providing a more reliable and robust measure of distance. In addition, Anderson and Luco (1983) found the distance measure used here to be analytically superior to the surface-distance measure proposed by Joyner and Boore (1981).

Site response is characterized by depth to basement rock,  $D$ . The importance of sediment depth in characterizing site amplification has been noted by many investigators, including Hanks (1975), Trifunac and Lee (1978, 1979), Rogers *et al.* (1985), Boore and Joyner (1984), King and Tucker (1984), Munguia and Brune (1984), Tucker and King (1984), Boore (1986, 1987), Campbell (1987, 1989a), Savy (1987), Aki (1988), Bard *et al.* (1988), Campillo *et al.* (1988), Silva *et al.* (1988), Kawase and Aki (1989), and Yamanaka *et al.* (1989). Where possible,  $D$  has been determined from velocity profiles derived from *in-situ* measurements (*e.g.*, refraction and reflection experiments) or from seismological studies conducted within the vicinity of the site (Wheeler, 1989, in press). However, when such measurements were not available, depths were inferred from gravity and aeromagnetic data, from stratigraphic sequences, and from slope extrapolation. For the majority of sites, basement was identified as the top of crystalline or metamorphic rock. However, in some cases (*e.g.*, parts of the Livermore Basin, California), basement—or what geophysicists often refer to as “seismic basement”—was found to be located within the sedimentary sequence. Such “basement” sediments are characterized by high *in-situ* velocities, low velocity gradients, and small velocity impedances.

### STRONG-MOTION DATA BASE

The strong-motion data base compiled for this study consists of near-source recordings from moderate-to-large earthquakes located throughout the world. The restriction to near-source distances— $R \leq 50$  km for  $M \geq 6.25$  and  $R \leq 30$  km for  $M < 6.25$ —was intended to minimize regional differences in anelastic attenuation while emphasizing those ground motions of greatest interest to earthquake engineers. Earthquakes were included only if they had seismogenic rupture within the shallow crust (depths shallower than about 25 km) in order to avoid potential differences in attenuation that might result from systematic differences in tectonic stresses and travel paths between deep and shallow earthquakes. Unlike other studies (*e.g.*, Joyner and Boore, 1981), shallow subduction earthquakes were included in the data base as a direct result of analyses by Boore (1986) and Youngs *et al.* (1988) which suggest that source processes and near-source ground motions are similar for shallow subduction and crustal earthquakes.



The data base compiled for this study (Appendix, Figs. 1-4) was modified from tabulations provided by Campbell (1981, 1987, 1989a). Because the Diablo Canyon power plant is sited on sedimentary rock, priority was given to strong-motion recordings on soft rock when selecting data to be added. Of particular note was the addition of strong-motion recordings from the 1972 Stone Canyon, Calif., earthquake ( $M_L = 4.7$ ), the 1976 Mesa de Andrade, Mexico, earthquake ( $M_L = 5.3$ ), the 1984 Morgan Hill, Calif., earthquake ( $M_S = 6.1$ ), the 1985 Central Chile earthquake ( $M_S = 7.8$ ), the 1986 North Palm Springs, Calif., earthquake ( $M_S = 6.0$ ), the 1986 Chalfant Valley, Calif., earthquake ( $M_S = 6.2$ ), and the 1987 Whittier Narrows, Calif., earthquake ( $M_L = 5.9$ ).

Strong-motion recordings were selected according to criteria proposed by Campbell (1987, 1989a), with the following exceptions. First, the magnitude 5.0 cutoff was relaxed to include processed recordings from the  $M_L = 4.7$  Stone Canyon earthquake, since a special aftershock study provided a reasonable basis for estimating the extent of seismogenic rupture during this earthquake. Second, as recommended by Campbell (1989a), soft-rock sites were included in order to provide recordings for site conditions similar to the Diablo Canyon site. Hard-rock sites were excluded based on analyses by Campbell (1986, 1989a) indicating that both the frequency content and amplitudes of recordings obtained on soft rock (primarily sedimentary rock) were substantially different from those obtained on hard rock (primarily crystalline rock). Third, shallow-soil sites—sites with 1-10 m of soil overlying rock—were excluded based on studies by Campbell (1987, 1988, 1989b) indicating that shallow soils can substantially amplify high-frequency components of ground motion.

## REGRESSION ANALYSES

Regression coefficients were determined from a weighted nonlinear regression analysis (Campbell, 1981, 1987, 1989a). The technique is based on algorithms developed by More *et al.* (1980). Weights were used to compensate for the potential bias associated with the uneven distribution of recordings between earthquakes. However, the weighting scheme was slightly modified from that originally proposed by Campbell (1981, 1987). The modification was intended to reduce the bias associated with having multiple recordings from a single earthquake at the same site location, since these recordings have virtually identical source, path, and site effects. Consistent with the old weighting scheme, recordings from a given earthquake that fall within a specified distance interval were assigned the same weight as those from other earthquakes within the same interval. In the new scheme, recordings from a given earthquake that occurred at the same site location are assigned the same cumulative weight as a single recording. As before, ten distance intervals were used to establish the weights, with these intervals having approximately equal logarithmic increments between 0 and 56.6 km.

The weight of each recording was computed from the following expression,

$$w_i = \frac{n/n_i}{\sum_{j=1}^n \frac{1}{n_j}}, \quad (2)$$



where  $i$  is the index of the recording;  $n_i = n_i^1 \cdot n_i^2$ ;  $n_i^1$  is the number of recordings from the same earthquake that produced the  $i^{\text{th}}$  recording that fall within the same distance interval;  $n_i^2$  is the number of recordings from the same earthquake that produced the  $i^{\text{th}}$  recording that occur at the same site location; and  $n$  is the total number of recordings. Note that the quantity  $n_i$  is not unique to a single recording; it is the same for all recordings from the same earthquake and site location that fall within the same distance interval. The above expression has been normalized to assure that the sum of the weights equals  $n$ , a constraint required in order to obtain a correct weighted estimate for the standard error,  $\sigma$ .

Other investigators have proposed different statistical methods to compensate for the potential bias associated with the uneven distribution of recordings between earthquakes. The two most notable are the two-step regression technique proposed by Joyner and Boore (1981) and the random-effects technique suggested by Brillinger and Preisler (1984). All three techniques are believed to give statistically similar results when the data are heteroscedastic.

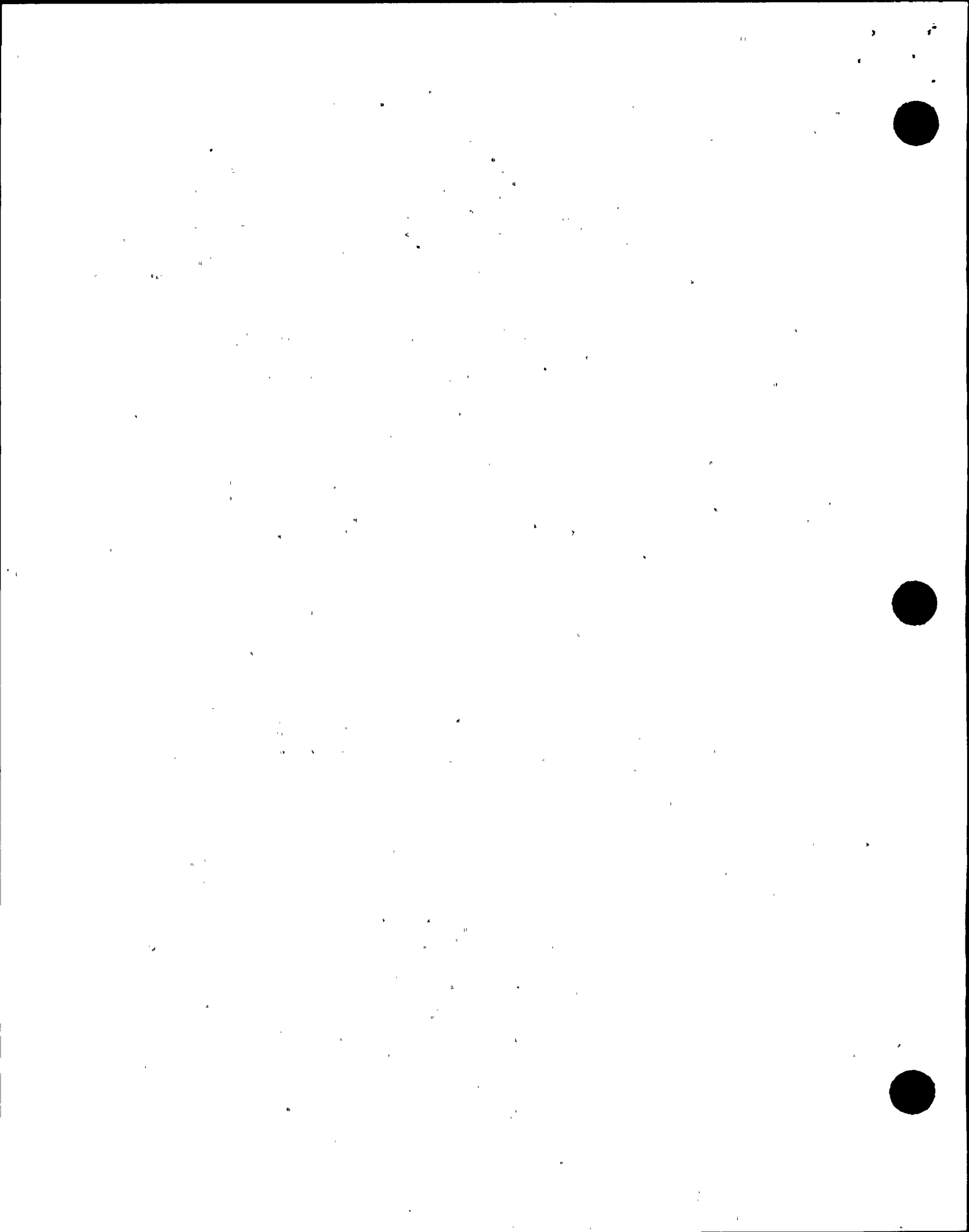
### Results for Peak Parameters

For the analysis of peak parameters, the regression coefficients  $a$ ,  $b$ ,  $c_i$ ,  $d$ ,  $e$ ,  $g_i$ , and  $h_i$  of Equation (1) were determined directly from the weighted nonlinear regression analysis described above; the results of which are summarized in Tables 1-3 and in Figures 5 and 6.

### Results for Response Spectra

Because of the multi-dimensional nature of pseudorelative velocity, the analysis of PSRV was considerably more complicated than the analysis of peak parameters. Campbell (1989a) found that independent regression analyses on the various spectral components led to unacceptably large period-to-period variability in the regression coefficients and predicted spectra. This variability is believed to have been caused by three factors: (1) the relatively large number of parameters included in the attenuation relationship, (2) the relatively small number of PSRV spectra available, and (3) period-to-period variability in the number of recordings.

When confronted with a similar result, Joyner and Boore (1982) and Joyner and Fumal (1985) chose to smooth their regression coefficients to obtain well-behaved spectra. However, several unique factors made this type of approach virtually impossible in the present analysis. First, some of the regression coefficients—most notably  $c_1$  and  $c_2$ —were found to be strongly correlated with one another, making it difficult to smooth them without extensive iteration. Second, the nonlinear form of Equation (1), together with the relatively large number of coefficients required to implement it, would have made it difficult to iterate during the smoothing process.



Therefore, rather than smooth the coefficients, the analysis was simplified by regressing on the ratio of PSRV to peak ground acceleration (PGA) rather than on PSRV itself—an approach first proposed by Newmark and Hall (1982) and latter adopted by many other investigators (*e.g.*, Sadigh, 1983; Campbell, 1985, 1989a; Joyner and Boore, 1988). Besides giving more stable results, the analysis of PSRV/PGA has several advantages that makes it suitable for developing spectral attenuation relationships: (1) it simplifies the analysis by reducing the number of coefficients to be evaluated (*e.g.*, now only  $a$ ,  $e$ ,  $f_i$ ,  $g_i$ , and  $h_i$  of Equation (1) need be evaluated, since the remaining coefficients are determined from the analysis of PGA), (2) it minimizes the impact of period-to-period variability in the number of recordings and (3) it inherits the reliability associated with the prediction of PGA.

The prediction of PSRV from PGA has been criticized to some degree in the literature (*e.g.*, Joyner and Boore, 1988; Bender and Campbell, 1989). The major criticism concerns the use of peak acceleration to scale a fixed spectral shape—an approach which neglects differences in the observed frequency dependence of PSRV on magnitude, distance, and site conditions. The attenuation relationship developed in the present study avoids such criticism by allowing PSRV/PGA to scale freely with each of these parameters.

In the previous analysis (Campbell, 1989a), there were too many regression coefficients to insure convergence of the nonlinear algorithms. Therefore, it was necessary to perform the analysis in several steps—each step concentrating on a different set of parameters—until all of the coefficients were determined. With each successive step, an analysis of residuals was used to validate the appropriateness of the regression coefficients determined in each of the previous steps. Campbell (1989a) compared the procedure to a stepwise regression analysis. In the present study, the regression analysis of  $\ln(\text{PSRV/PGA})$  could be done in a single step, since good starting values for the regression coefficients insured convergence during the iteration process.

Due to excessive variability, several of the regression coefficients were constrained to be independent of period. Coefficients  $f_2$  and  $g_2$  were constrained by regressing on all spectral values simultaneously—the equivalent of a multivariate multiple regression analysis (Johnson and Wichern, 1982). Coefficient  $f_3$  had to be arbitrarily constrained to a value of -4.7, when it became evident that its unconstrained absolute value, which was less than the smallest magnitude in the data base, predicted a negative correlation between  $\ln(\text{PSRV/PGA})$  and  $M$  for small-magnitude earthquakes. Inspection of the recordings indicated that this was caused by a low signal-to-noise ratio in the long-period components of the small-magnitude spectra, no doubt the result of improper processing. Because of this constraint, the PSRV attenuation relationships developed in this study are not valid for  $M \leq 4.7$ .

Attenuation relationships for  $\ln \text{PSRV}$  were derived by mathematically combining the regression results for  $\ln \text{PGA}$  and  $\ln(\text{PSRV/PGA})$  through the relationship,

$$\ln \text{PSRV} = \ln \text{PGA} + \ln(\text{PSRV/PGA}); \quad (3)$$



the results of which are summarized in Tables 1-3 and Figures 7 and 8.

As a final check on the results, standardized weighted residuals associated with the prediction of  $\ln$  PSRV were calculated and plotted against magnitude, distance, and depth to basement rock; and hypothesis tests on subsets of residuals were used to statistically verify the adequacy of Equation (1) in modelling the effects of site geology, style of faulting, and building size and embedment.

This analysis identified three trends worth noting. The first was a slight tendency for the residuals to be negatively correlated with distance at short periods and positively correlated with distance at long periods. This trend confirms previous observations that PSRV spectra attenuate more rapidly than PGA at short periods but less rapidly than PGA at long periods (*e.g.*, Joyner and Boore, 1982; Joyner and Fumal, 1985). However, with correlation coefficients less than 0.2, these trends are not significant at the near-source distances of interest in this study. Similar conclusions were offered by Silva and Green (1989), whose modelling studies indicated that response spectral shape is virtually independent of distance for distances less than about 50 km.

A second trend observed in the residuals was a tendency for the strike-slip vertical component of  $\ln$  PSRV to be strongly correlated with distance for  $T = 0.075-0.75$  sec and  $R < 12$  km. Taken at face value, this trend suggests that close-in strike-slip spectra have a bimodal shape. However, inspection of the spectra indicated that this behavior was being dominated by near-source recordings from the 1979 Imperial Valley earthquake (Brady *et al.*, 1980; Porter, 1983) and did not warrant further consideration at this time.

Finally, there was some indication in the residuals that  $K_1$  and  $K_2$  may be dependent on distance at short periods. A similar correlation was observed by Campbell (1987). However, further analysis indicated that this trend was being controlled by only a few recordings from the 1957 Daly City and 1971 San Fernando earthquakes and, as a result, was not considered significant enough to be included in the present analysis.

Since the attenuation relationships for  $\ln$  PSRV were developed by combining regression models for  $\ln$  PGA and  $\ln$  (PSRV/PGA), conventional standard errors of regression were not available. Instead, standard errors were computed directly from the weighted residuals, using the number of degrees of freedom,  $\nu = n - p$ , where  $n$  is the number of strong-motion recordings, and  $p$  is the number of regression coefficients in the model.

PG&E (1990) and Youngs *et al.* (1990) have demonstrated the importance of dividing the total uncertainty in the standard error into between-earthquake (inter-earthquake) variability and within-earthquake (intra-earthquake) variability. Once this is done, they find that the total uncertainty, represented by the square-root-sum-of-squares of the between-earthquake and within-earthquake variabilities decreases noticeably with earthquake magnitude.

In order to test this hypothesis in the present study, an analysis of residuals was used to compute between-earthquake variability ( $\sigma_b$ ), within-earthquake variability ( $\sigma_w$ ), and



total variability ( $\sigma_t$ ) for three magnitude intervals: 4.7-7.8, 4.7-6.1, 6.2-7.8. A smaller partitioning of the data did not seem warranted at this time due to the relatively small number of near-source recordings used in the present study. The results of this analysis are summarized in Tables 4 and 5. There are several trends worth noting in these tables. First, all standard errors, including the total standard error, are smaller for the larger magnitudes than they are for the smaller magnitudes, confirming the results of PG&E (1990) and Youngs *et al* (1990). Second, between-earthquake variability becomes relatively less important for large-magnitude earthquakes.

Although the computed standard errors for PSRV showed some serial correlation with period, they can be averaged over period to provide constant estimates of  $\sigma_t$  for purposes of computing a smooth median-plus-one-standard-deviation PSRV spectrum. The resulting average total standard errors for the three magnitude ranges 4.7-7.8, 4.7-6.1, and 6.2-7.8 are:  $0.516 \pm 0.030$ ,  $0.687 \pm 0.057$ , and  $0.434 \pm 0.061$  for the horizontal components, and  $0.653 \pm 0.056$ ,  $0.866 \pm 0.091$ , and  $0.562 \pm 0.088$  for the vertical components, respectively. Corresponding total standard errors for PHA, PVA, PHV, and PVV may be found in Tables 4 and 5.

### Significance of Results

Because of the nonlinear form of Equation (1), it is difficult to make specific statements concerning the statistical significance of the regression coefficients. A true test of significance requires a *Monte Carlo* simulation (Gallant, 1975); which, because of its complexity, could not be performed for all of the relationships developed in this study.

Campbell (1989a) performed a 1000-point *Monte Carlo* simulation to determine the significance of PHA regression coefficients  $a$ ,  $b$ ,  $c_1$ ,  $c_2$ ,  $d$ ,  $e$ ,  $h_1$ , and  $h_2$  in his study. The simulation demonstrated that all eight coefficients were significantly different from zero at the 90-percent confidence level. The equivalence of the two studies would suggest similar results in the present study.

### Soft-Rock Sites

Due to the small number of soft-rock recordings, an analysis of residuals was used to assess whether the attenuation relationships developed from the combined soil and soft-rock data were statistically adequate for predicting ground motions recorded on soft rock. In all cases, the hypothesis that the mean of the soil residuals are equal to the mean of the soft-rock residuals could not be rejected at the 90-percent confidence level. Therefore, it can be concluded that the near-source attenuation relationships developed in this study are appropriate for predicting near-source ground motions for both soil and soft-rock sites. This conclusion, however, may only be appropriate at near-source distances, where differences in ground motion due to site geology are known to be small.



## DISCUSSION OF RESULTS

### Ground-Motion Saturation

Both peak ground-motion parameters and short-period response spectra were found to "saturate" (*i.e.*, become independent of magnitude) at  $R = 0$ —the presumed source of radiated ground motion—as indicated by simple source theory (*e.g.*, Brune, 1970; Campbell, 1985). However, for  $T > 0.3$  sec, Equation (1) preempts complete saturation of PSRV by including a magnitude term that is independent of distance. This magnitude dependence, which increases with period up to a period of 2.0 sec, then slowly tapers off (see the behavior of  $f_1$  in Tables 1 and 2) is also consistent with simple source theory (*e.g.*, Aki, 1967; Brune, 1970).

### Style of Faulting

Ground motions from reverse faults were found to be larger than those from strike-slip faults. The effects, however, are substantially smaller than was found previously for soil recordings (Campbell, 1987, 1989a). The current results indicate a 24% increase in peak horizontal acceleration between reverse-slip and strike-slip events; whereas, Campbell (1989a), using an identical analysis for soil sites, found an increase of 47%. Why the inclusion of soft-rock recordings should have such an impact on this parameter is not known at this time. The large variability in this parameter may simply reflect the large amount of statistical uncertainty associated with its estimation. There were no normal-slip earthquakes included in the data base, so there was no basis with which to test McGarr's (1984) or Westaway and Smith's (1989) hypotheses regarding the effects of normal-slip earthquakes on ground motion.

### Building Effects

Building effects were found to be significant. Recordings from buildings greater than 2 stories in height were found to have smaller peak accelerations and smaller short-period response spectral ordinates, and larger peak velocities and larger long-period response spectral ordinates, than recordings from small buildings and free-field sites. However, unlike the approach taken by Campbell (1987), these effects were not modelled as being distance dependent. There was a tendency towards smaller short-period ground motions for large embedded buildings at small distances, but this effect was controlled by only a few recordings—notably those from the 1957 Daly City and 1971 San Fernando earthquakes—and, therefore, was not considered to be statistically significant. Likewise, the dependence of PHV on sediment depth, which Campbell (1987) found to depend on building size, was no longer found to be significantly correlated with building effects. The reader should be aware that the building effects modelled in the present study represent only a simple characterization of the complex soil-structure interaction (SSI) and embedment effects expected on the bases of analytical studies (*e.g.*, Wolf, 1985), and should not be used to model specific SSI or embedment effects. They are used here to provide a first-order adjustment to free-field site conditions and, thus, provide a more robust estimate of free-field ground motion.



## Source Directivity

Campbell (1987) included a parameter for source directivity based on three recordings that he believed were significantly amplified by a combination of site effects and source directivity. Each of these recordings had three factors in common: (1) unilateral rupture towards the recording site, (2) source-to-site azimuths that fell within 5-10 degrees of the direction of rupture, and (3) sediments over 5 km deep. These same recordings were found to have significantly higher ground motions in the present study as well. However, there has been a tendency among users to apply the previously developed "directivity" parameter—which Campbell (1987) suggests is a combination of near-maximum effects of both directivity and site amplification—to model the more common azimuthal effects normally ascribed to radiation pattern and simple source directivity. As a result, the directivity parameter proposed by Campbell (1987) was excluded from the present study. A precursory empirical analysis of simple source directivity, using recordings from several linear arrays, suggested that simple directivity effects may be present in the data; however, their modelling was beyond the scope of this study.

## Sediment Depth

Depth to basement rock was found to be important in amplifying peak velocity as well as horizontal and vertical response spectra for  $T \geq 1.0$  sec. The amplification increases rapidly with depth for small sediment depths and becomes relatively constant at greater depths. The increase of  $g_1$  with period (Tables 1 and 2) indicates that the amount of amplification increases with period as well, broadening the spectral shape at larger depths. This is quantitatively similar to results presented by Trifunac and Lee (1978, 1979) and Rogers *et al.* (1985), and is qualitatively consistent with the dependence of PSRV on shear-wave velocity found by Joyner and Fumal (1985).

## Distribution of Residuals

The total standard errors associated with PHA and PHV for the magnitude range 4.7-7.8 were found to be substantially larger than those estimated by Campbell (1987). Although part of this increase is due to the exclusion and simplification of parameters used to model source directivity and building effects, much of it can be attributed to increased dispersion associated with the added recordings. Also of note are the relatively large standard errors associated with the vertical components. Of direct importance to ground-motion estimation for large-magnitude earthquakes, was the finding that total variability, between-earthquake variability, and within-earthquake variability are all magnitude dependent, with each, especially between-earthquake variability, decreasing with increasing magnitude.

It is interesting to note that, in most cases, a chi-square test indicated that the distribution of residuals could be rejected as being Gaussian—equivalent to a lognormal distribution for the strong-motion parameter itself—at the 90-percent confidence level. The tendency is for a more peaked distribution of residuals than is expected from a Gaussian distribution. As a result, the common assumption of lognormality will tend to increase



the weight of the tails of the distribution and lead to an overestimation of ground motion at the upper fractiles. This overestimation can be avoided by making ground-motion estimates in terms of multiples of the standard error, as has been done in this report, without attempting to assign a specified fractile to the results.

## GROUND-MOTION ESTIMATES FOR DIABLO CANYON

The attenuation relationships described in the previous section were used to develop site-specific estimates of free-field ground motion at the Diablo Canyon site for the Long Term Seismic Program (LTSP) analysis earthquake proposed by PG&E. This earthquake is a moment magnitude ( $M_w$ ) 7.2 earthquake located about 4.5 km offshore on the Hosgri fault (PG&E, 1988).

There is some uncertainty associated with the actual location and geometry of the Hosgri fault. Based on an interpretation of geological and geophysical data, PG&E (1988) has proposed three possible faulting scenarios: strike-slip displacement on a vertical fault, reverse-oblique displacement on a steeply dipping fault, and thrusting on a shallow-dipping fault. Seismogenic distance, as defined in the present study, will be different for each of these scenarios. Based on a depth section and crustal velocity model provided by PG&E (1990), seismogenic distance to the Diablo Canyon site was estimated to be 4.7, 4.9, and 5.1 km for the reverse-oblique, strike-slip, and thrusting scenarios, respectively.

Seismic velocity profiles near the site (PG&E, 1988, Figs. 2-9, 4-13, and 5-5) infer a relatively strong velocity gradient within the shallow crust to a depth of approximately 4 km. Although rocks of the Franciscan Complex—usually considered to be basement rock—underlay the site at a depth of 1-2 km, the inferred velocity gradient in the upper 4 km is more representative of sedimentary rock than basement rock (R. Wheeler and K. Campbell, unpublished data). As a result, depth to basement rock was conservatively estimated to be 4 km for purposes of predicting ground motions at the Diablo Canyon site. This assumption, however, only affects estimates of peak velocity and response spectra for  $T \geq 1.0$  sec. It should be noted that PG&E did not include sediment depth as a parameter in their analyses.

Estimates of peak acceleration and peak velocity for PG&E's proposed LTSP analysis earthquake are presented in Table 4. In making these estimates,  $M_S$  was considered equivalent to  $M_w$  (Hanks and Kanamori, 1979); and the standard error, as represented by the total standard error,  $\sigma_t$ , for the magnitude range 6.2-7.8, was taken from Tables 4 and 5. For convenience, the estimates have been segregated by style of faulting and uncertainty level.

Estimates for the reverse-oblique and thrust scenarios have been increased by the style-of-faulting factor developed during this study (Tables 1 and 2), since, by definition, both are reverse faults. These factors, which represent the increase in ground motion over that expected for strike-slip faulting, are 24% for PHA and PSRVH, 12% for PVA and PSRVV, 11% for PHV, and 23% for PVV. PG&E (1988), on the other hand, has adopted



a different style-of-faulting factor for each of the above faulting scenarios. Their factors are 10% for reverse-oblique faulting and 20% for the thrust faulting.

If ground-motion estimates for each type of fault are combined according to the weighting scheme proposed by PG&E (1988)—a weight of 0.65 for strike-slip faulting, a weight of 0.30 for reverse-oblique faulting, and a weight of 0.05 for thrust faulting—the weighted median and median-plus-one-standard-deviation (median+1 $\sigma$ ) estimates for PHA and PHV are 0.55g, 0.82g, 59.2 cm/sec, and 88.6 cm/sec, respectively; and for PVA and PVV are 0.53g, 0.86g, 24.3 cm/sec, and 40.7 cm/sec.

Five-percent damped pseudoabsolute acceleration (PSAA) spectra for PG&E's proposed LTSP analysis earthquake, estimated separately for each of the three proposed fault scenarios, are presented in Figures 9–14. For this purpose, the standard error was taken as the period invariant total standard error,  $\sigma_t$ , for the magnitude range 6.2–7.8, as derived in a previous section. These spectra may be compared with similar spectra provided by PG&E (1988; Figs. 4-22 through 4-26).

## REFERENCES

- Aki, K. (1967). Scaling law of seismic spectrum, *J. Geophys. Res.*, v. 72, p. 1217–1231.
- Aki, K. (1988). Local site effects on strong ground motion, in Von Thun, J.L., editor, *Proceedings, Conference on Earthquake Engineering and Soil Dynamics II—Recent Advances in Ground-Motion Evaluation*, A.S.C.E. Geotechnical Special Publication No. 20, p. 103-155.
- Anderson, J.G., and J.E. Luco (1983). Parametric study of near-field ground motions for oblique-slip and dip-slip dislocation models, *Bull. Seism. Soc. Am.*, v. 73, p. 45–57.
- Bard, P.-Y., M. Campillo, F.J. Chavez-Garcia, and F. Sanchez-Sesma (1988). The Mexico earthquake of September 19, 1985—A theoretical investigation of large- and small-scale amplification effects in the Mexico City Valley, *Earthquake Spectra*, v. 4, p. 609–633.
- Bender, B., and K.W. Campbell (1989). A note on the selection of minimum magnitude for use in seismic hazard analysis, *Bull. Seism. Soc. Am.*, v. 79, p. 199–204.
- Boore, D.M. (1986). Short-period P- and S-wave radiation from large earthquakes, *Bull. Seism. Soc. Am.*, v. 76, p. 43–64.
- Boore, D.M. (1987). The prediction of strong ground motion, in *Strong Ground Motion Seismology*, Erdik, M., and M.N. Toksoz, editors, NATO Advanced Studies Institute Series, D. Reidel Publishing Co., Dordrecht, The Netherlands, p. 109–141.
- Boore, D.M., and W.B. Joyner (1982). The empirical prediction of ground motion, *Bull. Seism. Soc. Am.*, v. 72, p. S43–S60.



Boore, D.M., and W.B. Joyner (1984). Ground motions and response spectra at soil sites from seismological models of radiated spectra, in *Proceedings, Eighth World Conference on Earthquake Engineering*, San Francisco, 1987, v. II, p. 457-464.

Brady, A.G., V. Perez, and P.N. Mork (1980). The Imperial Valley earthquake, October 15, 1979—Digitization and processing of accelerograph records, *U. S. Geological Survey Open-File Report 80-703*.

Brillinger, D.R., and H.K. Preisler (1984). An exploratory analysis of the Joyner-Boore attenuation data, *Bull. Seism. Soc. Am.*, v. 74, p. 1441-1450.

Brune, J.N. (1970). Tectonic stress and the spectra of seismic shear waves from earthquakes, *J. Geophys. Res.*, v. 75, p. 4997-5009.

Campbell, K.W. (1981). Near-source attenuation of peak horizontal acceleration, *Bull. Seism. Soc. Am.*, v. 71, p. 2039-2070.

Campbell, K.W. (1982). Near-source scaling characteristics of peak horizontal acceleration for moderate-to-large earthquakes, in *Proceedings, Conference XVI—A Workshop on the Dynamic Characteristics of Faulting Inferred from Recordings of Strong Ground Motion*, Incline Village, Calif., 1981, U. S. Geological Survey Open-File Report 82-591, v. 1, p. 120-184.

Campbell, K.W. (1985). Strong motion attenuation relations: A ten-year perspective, *Earthquake Spectra*, v. 1, p. 759-804.

Campbell, K.W. (1986). An empirical estimate of near-source ground motion for a major,  $m_b = 6.8$ , earthquake in the Eastern United States, *Bull. Seism. Soc. Am.*, v. 76, p. 1-17.

Campbell, K.W. (1987). Predicting strong ground motion in Utah, in Gori, P.L., and Hays, W.W., editors, *Assessment of Regional Earthquake Hazards and Risk Along the Wasatch Front, Utah*, U. S. Geological Survey Open-File Report 87-585, v. II, p. L1-L90.

Campbell, K.W. (1988). Comment on "An investigation into earthquake ground motion characteristics in Eastern North America" by G.R. Toro and R.K. McGuire, *Bull. Seism. Soc. Am.*, v. 78, p. 2098-2101.

Campbell, K.W. (1989a). Empirical prediction of near-source ground motion for the Diablo Canyon power plant site, San Luis Obispo County, California, *U. S. Geological Survey Open-File Report 89-484*, 115 p.

Campbell, K.W. (1989b). The dependence of peak horizontal acceleration on magnitude, distance, and site effects for small-magnitude earthquakes in California and Eastern North America, *Bull. Seism. Soc. Am.*, v. 79, p. 1311-1346.



- Campillo, C., P.-Y. Bard, F. Nicollin, and F. Sanchez-Sesma (1988). The Mexico earthquake of September 19, 1985—The incident wavefield in Mexico City during the great Michoacan earthquake and its interaction with the deep basin, *Earthquake Spectra*, v. 4, p. 591-608.
- Esteva, L. (1970). Seismic risk and seismic design decisions, in Hanson, R.J., editor, *Seismic design for nuclear power plants*, M.I.T. Press, Cambridge, Mass., p. 142-182.
- Gallant, A.R. (1975). Nonlinear regression, *The American Statistician*, v. 29, p. 73-81.
- Hadley, D.M., D.V. Helmberger, and J.A. Orcutt (1982). Peak acceleration scaling studies, *Bull. Seism. Soc. Am.*, v. 72, p. 959-979.
- Hanks, T.C. (1975). Strong ground motion of the San Fernando, California, earthquake—Ground displacements, *Bull. Seism. Soc. Am.*, v. 65, p. 93-226.
- Hanks, T.C., and H. Kanamori (1979). A moment magnitude scale, *J. Geophys. Res.*, v. 84, p. 2348-2350.
- Johnson, R.A., and D.W. Wichern (1982). *Applied multivariate statistical analysis*, Prentice Hall, Inc., Englewood Cliffs, New Jersey.
- Joyner, W.B., and D.M. Boore (1981). Peak horizontal acceleration and velocity from strong-motion records including records from the 1979 Imperial Valley, California, earthquake, *Bull. Seism. Soc. Am.*, v. 71, p. 2011-2038.
- Joyner, W.B., and D.M. Boore (1982). Prediction of earthquake response spectra, *U. S. Geological Survey Open-File Report 82-977*.
- Joyner, W.B., and D.M. Boore (1988). Measurement, characterization, and prediction of strong ground motion, in Von Thun, J.L., editor, *Proceedings, Conference on Earthquake Engineering and Soil Dynamics II—Recent Advances in Ground-Motion Evaluation*, A.S.C.E. Geotechnical Special Publication No. 20, p. 43-102.
- Joyner, W.B., and T.E. Fumal (1985). Predictive mapping of earthquake ground motion, in Ziony, J.I., editor, *Evaluating Earthquake Hazards in the Los Angeles Region—An Earth Science Perspective*, U. S. Geological Survey Professional Paper 1360, p. 203-220.
- Kawase, H., and K. Aki (1989). A study on the response of a soft basin for incident S, P, and Rayleigh waves with special reference to the long duration observed in Mexico City, *Bull. Seism. Soc. Am.*, v. 79, p. 1361-1382.
- King, J.L., and B.E. Tucker (1984). Observed variations of earthquake motion across a sediment-filled valley, *Bull. Seism. Soc. Am.*, v. 74, p. 137-151.



McGarr, A. (1984). Scaling of ground motion parameters, state of stress and focal depth, *J. Geophys. Res.*, v. 89, p. 6969-6979.

More, J.J., B.S. Garbow, and K.E. Hillstrom (1980). User guide for MINPACK-1, *Argonne National Laboratory Report ANL-80-74*.

Munguia, L., and J.N. Brune (1984). Local magnitude and sediment amplification observations from earthquakes in the Northern Baja-Southern California region, *Bull. Seism. Soc. Am.*, v. 74, p. 107-119.

Newmark, N.M., and W.J. Hall (1982). *Earthquake spectra and design*, Earthquake Engineering Research Institute, Berkeley, Calif.

PG&E (1988). Final report of the Diablo Canyon long term seismic program for the Diablo Canyon power plant, Pacific Gas and Electric Company report to the U. S. Nuclear Regulatory Commission, Docket Nos. 50-275 and 50-323, July 31, 1988, San Francisco, Calif.

PG&E (1990). Response to ground-motion questions LP 1 and LP 9, and workshop questions 1 through 6, Pacific Gas and Electric Company report to the U.S. Nuclear Regulatory Commission, Docket Nos. 50-275 and 50-323, August, 1990, San Francisco, Calif.

Porter, L.D. (1983). Processed data from the strong-motion records of the Imperial Valley earthquake of October 15, 1979, *California Division of Mines and Geology Special Publication 65*.

Rogers, A.M., J.C. Tinsley, and R.D. Borcherdt (1985). Predicting relative ground response, in Ziony, J.I., editor, *Evaluating Earthquake Hazards in the Los Angeles Region—An Earth Science Perspective*, U. S. Geological Survey Professional Paper 1360, p. 221-248.

Sadigh, K. (1983). Considerations in the development of site-specific spectra, in *Proceedings, Conference XXII—A Workshop on Site-Specific Effects of Soil and Rock on Ground Motion and the Implications for Earthquake-Resistant Design*, Santa Fe, New Mexico, 1983, U. S. Geological Survey Open-File Report 83-845, p. 423-458.

Savy, J.B., D.L. Bernreuter, and J.C. Chen (1987). A methodology to correct for effect of the local site characteristics in seismic hazard analyses, in *Ground Motion and Engineering Seismology*, Cakmak, A.S., editor, *Developments in Geotechnical Engineering Vol. 44*, Elsevier, Amsterdam, p. 243-255.

Shakál, A.F., and D.L. Bernreuter (1981). Empirical analysis of near-source ground motion, *U. S. Nuclear Regulatory Commission Report NUREG/CR-2095*.



- Silva, W.J., and R.K. Green (1989). Magnitude and distance scaling of response spectral shapes for rock sites with applications to North American tectonic environment, *Earthquake Spectra*, v. 5, p. 591-624.
- Silva, W., T. Turcotte, and Y. Moriwaki (1984). Soil response to earthquake ground motion, *Electric Power Research Institute Report NP-5747*.
- Trifunac, M.D., and V.W. Lee (1978). Dependence of the Fourier amplitude spectra of strong motion acceleration on the depth of sedimentary deposits, *University of Southern California Department of Civil Engineering Report CE78-14*.
- Trifunac, M.D., and V.W. Lee (1979). Dependence of pseudo-relative velocity spectra of strong motion acceleration on the depth of sedimentary deposits, *University of Southern California Department of Civil Engineering Report CE79-02*.
- Tucker, B.E., and J.L. King (1984). Dependence of sediment-filled valley response on input amplitude and valley properties, *Bull. Seism. Soc. Am.*, v. 74, p. 153-165.
- Westaway, R., and R.B. Smith (1989). Strong ground motion in normal-faulting earthquakes, *Geophys. J.*, v. 96, p. 529-559.
- Wheeler, R. (1989). Site geology and depth to basement rock at accelerograph stations that recorded the Morgan Hill, California, Earthquake, *U. S. Geological Survey Open-File Report* (in press).
- Wolf, J.P. (1985). *Dynamic soil-structure interaction*, Prentice-Hall, Inc., Englewood Cliffs, New Jersey.
- Yamanaka, H., K. Seo, and T. Samano (1989). Effects of sedimentary layers on surface-wave propagation, *Bull. Seism. Soc. Am.*, v. 79, p. 631-644.
- Youngs, R.R., S.M. Day, and J.L. Stevens (1988). Near field ground motions on rock for large subduction earthquakes, in Von Thun, J.L., editor, *Proceedings, Conference on Earthquake Engineering and Soil Dynamics II—Recent Advances in Ground-Motion Evaluation*, A.S.C.E. Geotechnical Special Publication No. 20, p. 445-462.
- Youngs, R.R., F. Makdisi, and K. Sadigh (1990). The case for magnitude dependent dispersion in peak ground acceleration [abs.], *Seismological Research Letters*, v. 61, p. 30.



**TABLE 1**  
Regression Coefficients: Horizontal Components

Parameter, Y	Period (sec)	No. Eq.	No. Rec.	a	b	c <sub>1</sub>	c <sub>2</sub>	d	e	f <sub>1</sub>	f <sub>2</sub>	f <sub>3</sub>	g <sub>1</sub>	g <sub>2</sub>
PHA, g	—	28	244	-2.245	1.09	0.361	0.576	-1.89	0.218	—	—	—	—	—
PHV, cm/sec	—	21	175	-1.765	1.38	0.0203	0.958	-1.44	0.101	—	—	—	0.529	0.471
PSRVH, cm/sec	0.04	16	99	-0.402	1.09	0.361	0.576	-1.89	0.218	—	—	—	—	—
	0.05	21	164	-0.141	1.09	0.361	0.576	-1.89	0.218	—	—	—	—	—
	0.075	21	167	0.489	1.09	0.361	0.576	-1.89	0.218	—	—	—	—	—
	0.10	21	167	0.987	1.09	0.361	0.576	-1.89	0.218	—	—	—	—	—
	0.15	21	167	1.625	1.09	0.361	0.576	-1.89	0.218	—	—	—	—	—
	0.20	21	167	1.988	1.09	0.361	0.576	-1.89	0.218	—	—	—	—	—
	0.30	21	167	2.370	1.09	0.361	0.576	-1.89	0.218	—	—	—	—	—
	0.40	21	167	2.153	1.09	0.361	0.576	-1.89	0.218	0.514	0.659	-4.7	—	—
	0.50	21	167	2.086	1.09	0.361	0.576	-1.89	0.218	0.738	0.659	-4.7	—	—
	0.75	21	167	1.802	1.09	0.361	0.576	-1.89	0.218	1.23	0.659	-4.7	—	—
	1.0	21	167	1.398	1.09	0.361	0.576	-1.89	0.218	1.59	0.659	-4.7	0.183	0.574
	1.5	21	167	0.795	1.09	0.361	0.576	-1.89	0.218	1.98	0.659	-4.7	0.488	0.574
	2.0	21	167	0.411	1.09	0.361	0.576	-1.89	0.218	2.23	0.659	-4.7	0.634	0.574
	3.0	20	155	-0.140	1.09	0.361	0.576	-1.89	0.218	2.39	0.659	-4.7	0.836	0.574
4.0	19	147	-0.188	1.09	0.361	0.576	-1.89	0.218	2.03	0.659	-4.7	1.17	0.574	

**TABLE 2**  
Regression Coefficients: Vertical Components

Parameter, Y	Period (sec)	No. Eq.	No. Rec.	a	b	c <sub>1</sub>	c <sub>2</sub>	d	e	f <sub>1</sub>	f <sub>2</sub>	f <sub>3</sub>	g <sub>1</sub>	g <sub>2</sub>
PVA, g	—	25	239	-3.829	0.991	0.0790	0.661	-1.50	0.111	—	—	—	—	—
PVV, cm/sec	—	21	172	-3.914	1.45	0.00394	1.17	-1.24	0.205	—	—	—	0.462	2.68
PSRVV, cm/sec	0.04	16	98	-1.901	0.991	0.0790	0.661	-1.50	0.111	—	—	—	—	—
	0.05	21	162	-1.465	0.991	0.0790	0.661	-1.50	0.111	—	—	—	—	—
	0.075	21	164	-0.722	0.991	0.0790	0.661	-1.50	0.111	—	—	—	—	—
	0.10	21	164	-0.304	0.991	0.0790	0.661	-1.50	0.111	—	—	—	—	—
	0.15	21	164	0.054	0.991	0.0790	0.661	-1.50	0.111	—	—	—	—	—
	0.20	21	164	0.263	0.991	0.0790	0.661	-1.50	0.111	—	—	—	—	—
	0.30	21	164	0.388	0.991	0.0790	0.661	-1.50	0.111	—	—	—	—	—
	0.40	21	164	0.290	0.991	0.0790	0.661	-1.50	0.111	0.181	0.711	-4.7	—	—
	0.50	21	164	0.055	0.991	0.0790	0.661	-1.50	0.111	0.463	0.711	-4.7	—	—
	0.75	21	164	0.014	0.991	0.0790	0.661	-1.50	0.111	0.669	0.711	-4.7	—	—
	1.0	21	164	-0.420	0.991	0.0790	0.661	-1.50	0.111	1.13	0.711	-4.7	0.177	0.513
	1.5	21	163	-1.012	0.991	0.0790	0.661	-1.50	0.111	1.62	0.711	-4.7	0.568	0.513
	2.0	21	163	-1.241	0.991	0.0790	0.661	-1.50	0.111	1.65	0.711	-4.7	0.613	0.513
	3.0	20	146	-1.451	0.991	0.0790	0.661	-1.50	0.111	1.28	0.711	-4.7	1.07	0.513
4.0	17	142	-1.536	0.991	0.0790	0.661	-1.50	0.111	1.15	0.711	-4.7	1.26	0.513	



**TABLE 3**  
Regression Coefficients: Building Effects

Horizontal Components					Vertical Components				
Parameter, Y	Period (sec)	$h_1$	$h_2$	$h_3$	Parameter, Y	Period (sec)	$h_1$	$h_2$	$h_3$
PHA, g	—	-0.137	-0.403	—	PVA, g	—	—	-0.337	—
PHV, cm/sec	—	0.093	—	0.219	PVV, cm/sec	—	0.276	-0.108	0.405
PSRVH, cm/sec	0.04	-0.137	-0.403	—	PSRVV, cm/sec	0.04	—	-0.337	-0.109
	0.05	-0.137	-0.403	—		0.05	-0.113	-0.645	-0.255
	0.075	-0.137	-0.403	—		0.075	-0.205	-0.529	-0.379
	0.10	-0.137	-0.403	—		0.10	-0.227	-0.588	-0.313
	0.15	-0.137	-0.403	—		0.15	—	-0.337	—
	0.20	-0.137	-0.403	—		0.20	—	-0.337	—
	0.30	-0.137	-0.403	—		0.30	—	-0.337	—
	0.40	-0.137	-0.403	—		0.40	—	-0.220	—
	0.50	-0.137	-0.403	—		0.50	—	0.0	—
	0.75	-0.137	-0.403	—		0.75	—	-0.191	—
	1.0	-0.137	-0.130	—		1.0	—	-0.123	—
	1.5	-0.137	0.118	—		1.5	—	0.338	0.589
	2.0	-0.137	0.091	—		2.0	—	0.402	0.963
	3.0	0.312	0.430	0.794		3.0	0.505	0.845	1.14
	4.0	0.394	0.515	0.892		4.0	0.602	1.04	1.23

**TABLE 4**  
Standard Errors: Horizontal Components

Parameter, Y	Period (sec)	Magnitude Range														
		4.7-7.8					4.7-6.1					6.2-7.8				
		No. Eq.	No. Rec.	$\sigma_t$	$\sigma_b$	$\sigma_w$	No. Eq.	No. Rec.	$\sigma_t$	$\sigma_b$	$\sigma_w$	No. Eq.	No. Rec.	$\sigma_t$	$\sigma_b$	$\sigma_w$
PHA, g	—	26	244	0.450	0.254	0.371	14	122	0.517	0.308	0.416	12	122	0.387	0.193	0.336
PHV, cm/sec	—	21	175	0.454	0.267	0.368	10	66	0.567	0.332	0.460	11	109	0.403	0.237	0.325
PSRVH, cm/sec	0.04	16	99	0.491	0.352	0.342	7	34	0.716	0.455	0.553	9	65	0.387	0.312	0.228
	0.05	21	164	0.532	0.386	0.365	10	62	0.631	0.408	0.482	11	102	0.492	0.390	0.301
	0.075	21	167	0.528	0.350	0.396	10	62	0.703	0.488	0.506	11	106	0.430	0.261	0.342
	0.10	21	167	0.526	0.349	0.394	10	62	0.703	0.495	0.500	11	105	0.427	0.254	0.343
	0.15	21	167	0.555	0.343	0.437	10	62	0.754	0.474	0.587	11	105	0.440	0.263	0.352
	0.20	21	167	0.532	0.299	0.440	10	62	0.722	0.406	0.598	11	105	0.421	0.237	0.348
	0.30	21	167	0.456	0.256	0.378	10	62	0.597	0.311	0.510	11	105	0.382	0.233	0.302
	0.40	21	167	0.464	0.245	0.394	10	62	0.671	0.355	0.569	11	105	0.342	0.179	0.291
	0.50	21	167	0.483	0.254	0.412	10	62	0.722	0.390	0.608	11	105	0.330	0.161	0.288
	0.75	21	167	0.548	0.319	0.446	10	62	0.776	0.480	0.609	11	105	0.420	0.211	0.363
	1.0	21	167	0.532	0.354	0.397	10	62	0.751	0.451	0.600	11	105	0.426	0.321	0.280
	1.5	21	167	0.530	0.341	0.405	10	62	0.687	0.387	0.567	11	105	0.478	0.344	0.333
	2.0	21	167	0.505	0.310	0.400	10	62	0.591	0.343	0.481	11	105	0.496	0.313	0.384
	3.0	20	155	0.520	0.310	0.417	9	50	0.628	0.431	0.457	11	105	0.520	0.276	0.442
	4.0	19	147	0.535	0.326	0.424	8	42	0.647	0.414	0.497	11	105	0.532	0.296	0.442



**TABLE 5**  
Standard Errors: Vertical Components

Parameter, Y	Period (sec)	Magnitude Range														
		4.7-7.8					4.7-6.1					6.2-7.8				
		No. Eq.	No. Rec.	$\sigma_t$	$\sigma_b$	$\sigma_w$	No. Eq.	No. Rec.	$\sigma_t$	$\sigma_b$	$\sigma_w$	No. Eq.	No. Rec.	$\sigma_t$	$\sigma_b$	$\sigma_w$
PVA, g	—	25	239	0.575	0.358	0.450	13	119	0.668	0.411	0.527	12	120	0.476	0.295	0.374
PVV, cm/sec	—	21	172	0.543	0.383	0.385	10	65	0.632	0.436	0.457	11	107	0.517	0.369	0.362
PSRVV, cm/sec	0.04	16	98	0.745	0.628	0.400	7	33	0.957	0.630	0.720	9	65	0.685	0.661	0.179
	0.05	21	162	0.715	0.531	0.479	10	61	0.991	0.674	0.726	11	101	0.554	0.464	0.303
	0.075	21	164	0.661	0.437	0.496	10	61	0.909	0.556	0.720	11	103	0.525	0.385	0.357
	0.10	21	164	0.631	0.409	0.480	10	61	0.905	0.544	0.724	11	103	0.464	0.342	0.314
	0.15	21	164	0.641	0.406	0.496	10	61	0.870	0.505	0.708	11	103	0.501	0.355	0.354
	0.20	21	164	0.590	0.391	0.442	10	61	0.761	0.432	0.626	11	103	0.498	0.383	0.319
	0.30	21	164	0.578	0.434	0.382	10	61	0.743	0.531	0.519	11	103	0.491	0.389	0.298
	0.40	21	164	0.602	0.443	0.407	10	61	0.789	0.413	0.314	11	103	0.519	0.413	0.314
	0.50	21	164	0.589	0.459	0.368	10	61	0.827	0.631	0.534	11	103	0.458	0.370	0.270
	0.75	21	164	0.603	0.491	0.350	10	61	0.808	0.422	0.272	11	103	0.502	0.422	0.272
	1.0	21	164	0.630	0.496	0.388	10	61	0.832	0.639	0.532	11	103	0.545	0.439	0.322
	1.5	21	163	0.715	0.579	0.421	10	60	0.939	0.745	0.572	11	103	0.634	0.522	0.361
	2.0	21	163	0.665	0.511	0.425	10	60	0.764	0.551	0.530	11	103	0.666	0.532	0.400
	3.0	20	146	0.718	0.491	0.524	9	43	1.050	0.659	0.817	11	103	0.650	0.469	0.450
	4.0	17	138	0.716	0.396	0.597	6	35	0.845	0.288	0.795	11	103	0.732	0.416	0.602

**TABLE 6**  
Site-Specific Estimates of Strong Ground Motion:  
Diablo Canyon Site, California  
( $M_S = 7.2$ ,  $R = 4.7-5.1$  km,  $D = 4$  km)

Parameter, Y	Strike Slip		Reverse Oblique		Thrust	
	Median	Median+1 $\sigma$	Median	Median+1 $\sigma$	Median	Median+1 $\sigma$
PHA, g	0.51	0.75	0.64	0.94	0.62	0.91
PVA, g	0.51	0.82	0.59	0.95	0.50	0.80
PHV, cm/sec	56.9	85.1	63.7	95.3	62.2	93.1
PVV, cm/sec	22.4	37.6	27.8	46.6	27.2	45.6



# PEAK ACCELERATION (Soil)

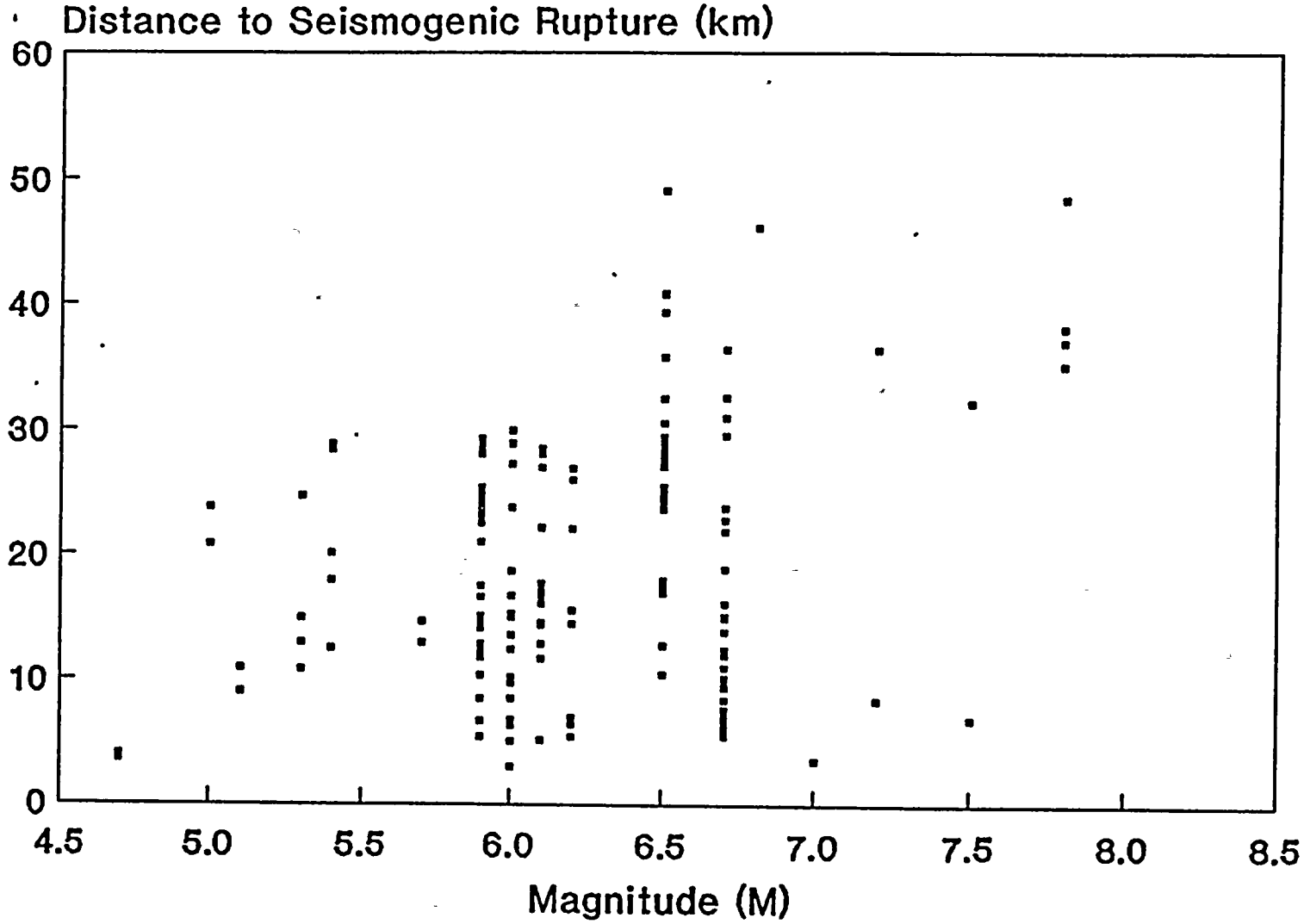


Fig. 1--Magnitude versus distance



# PEAK ACCELERATION (Soft Rock)

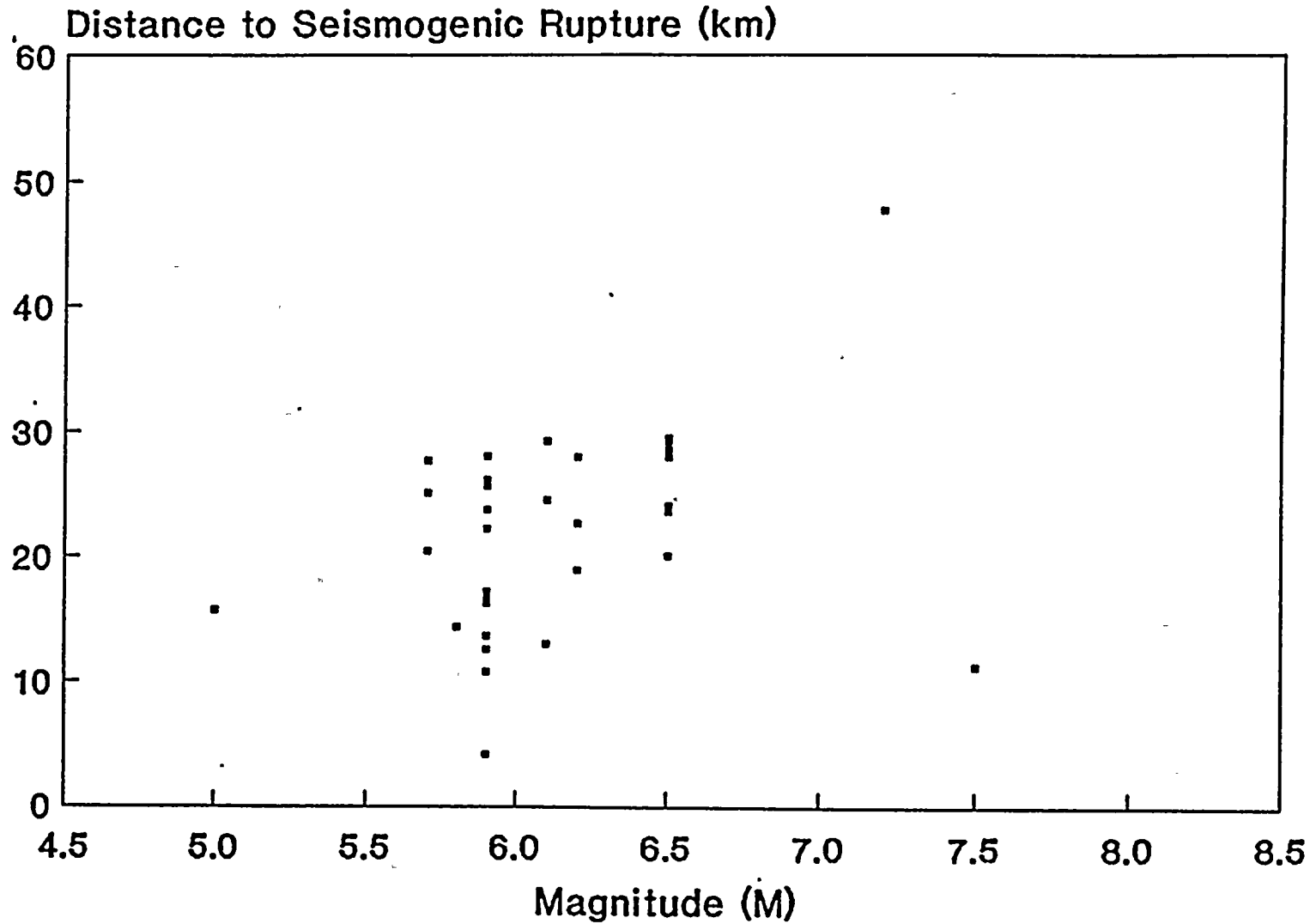


Fig. 2--Magnitude versus distance



# PEAK VELOCITY (Soil)

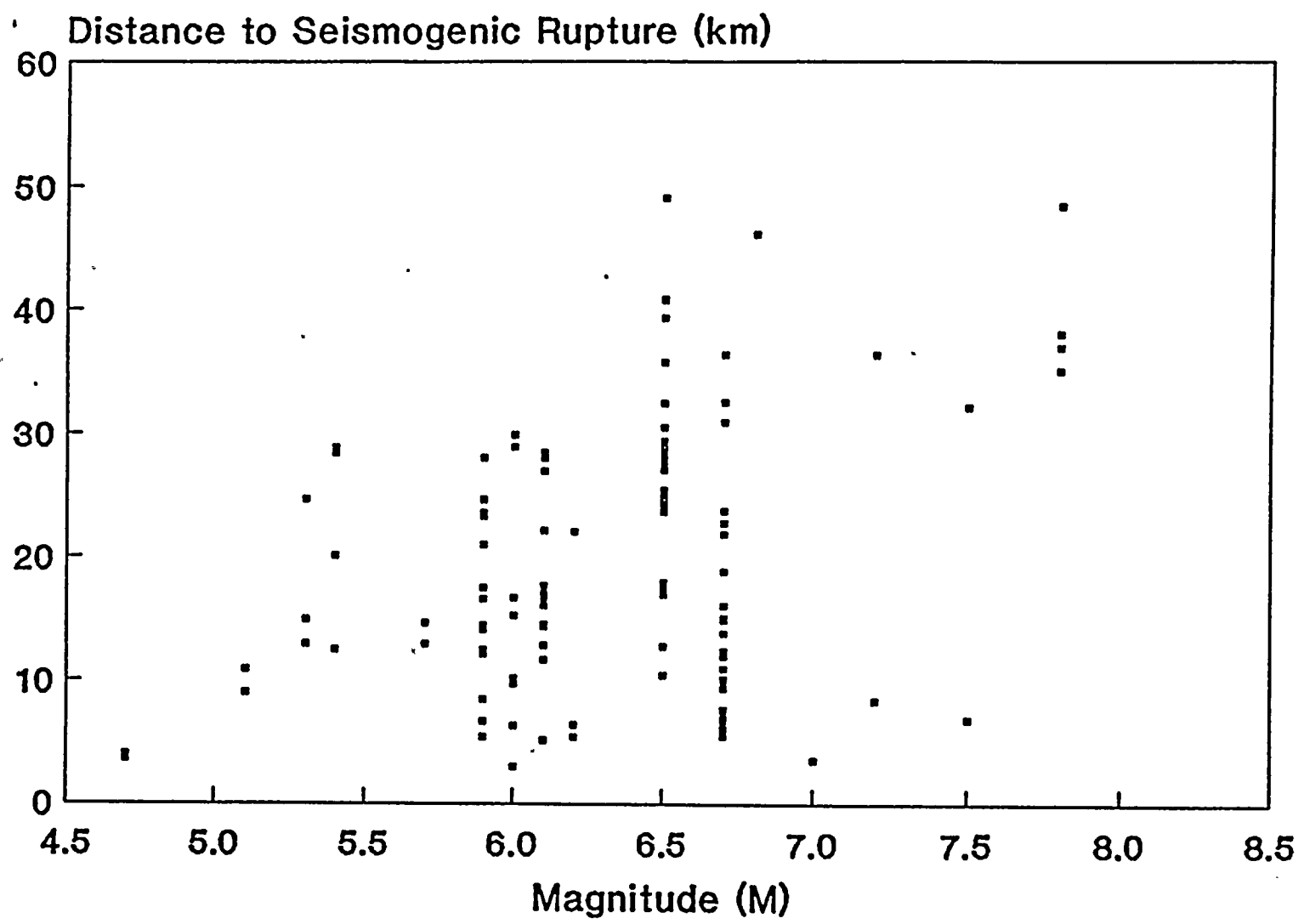
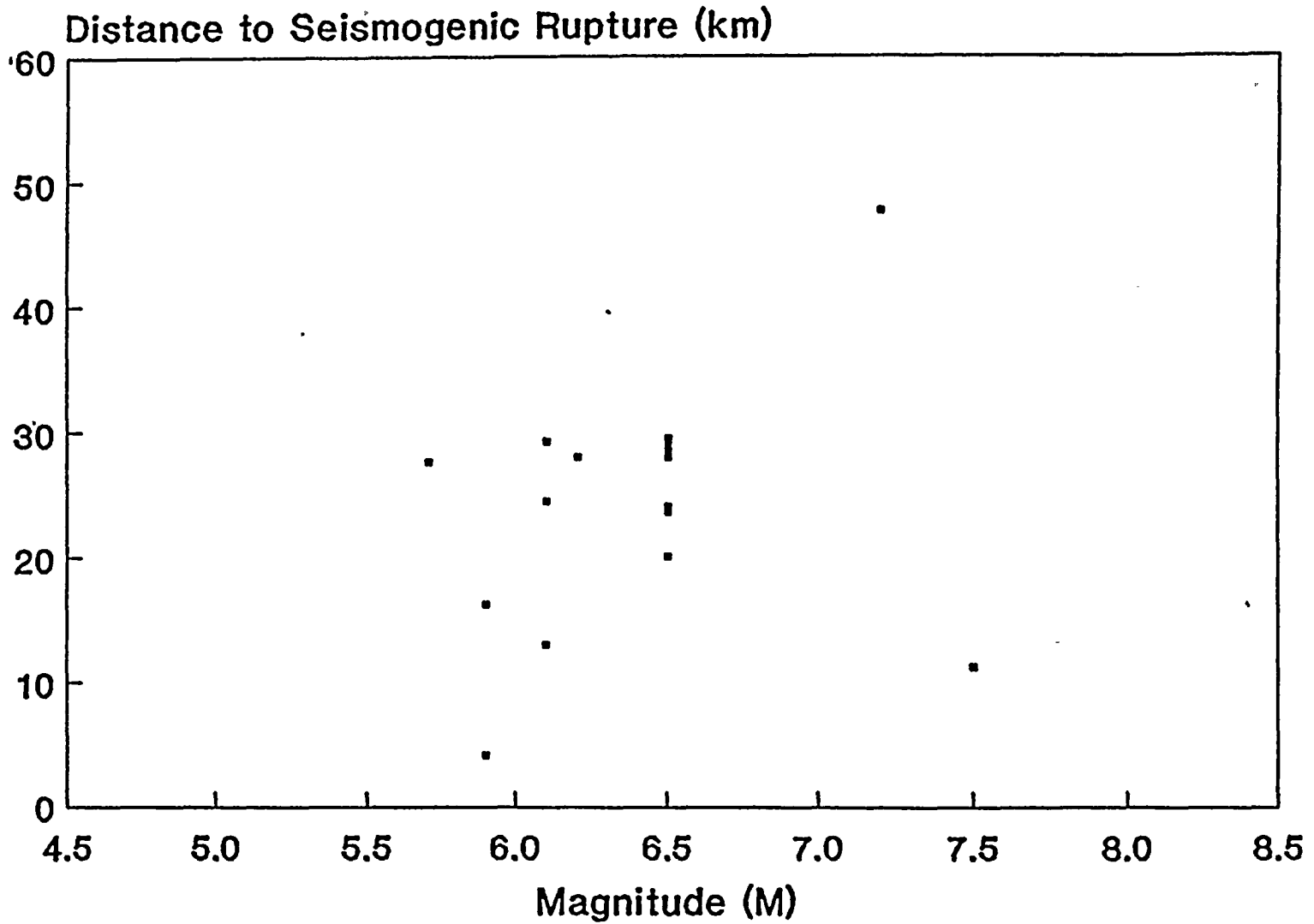


Fig. 3--Magnitude versus distance



# PEAK VELOCITY (Soft Rock)



23

Fig. 4--Magnitude versus distance



# PEAK ACCELERATION

Strike-Slip Faults;  $M = 5.0, 6.5, 8.0$

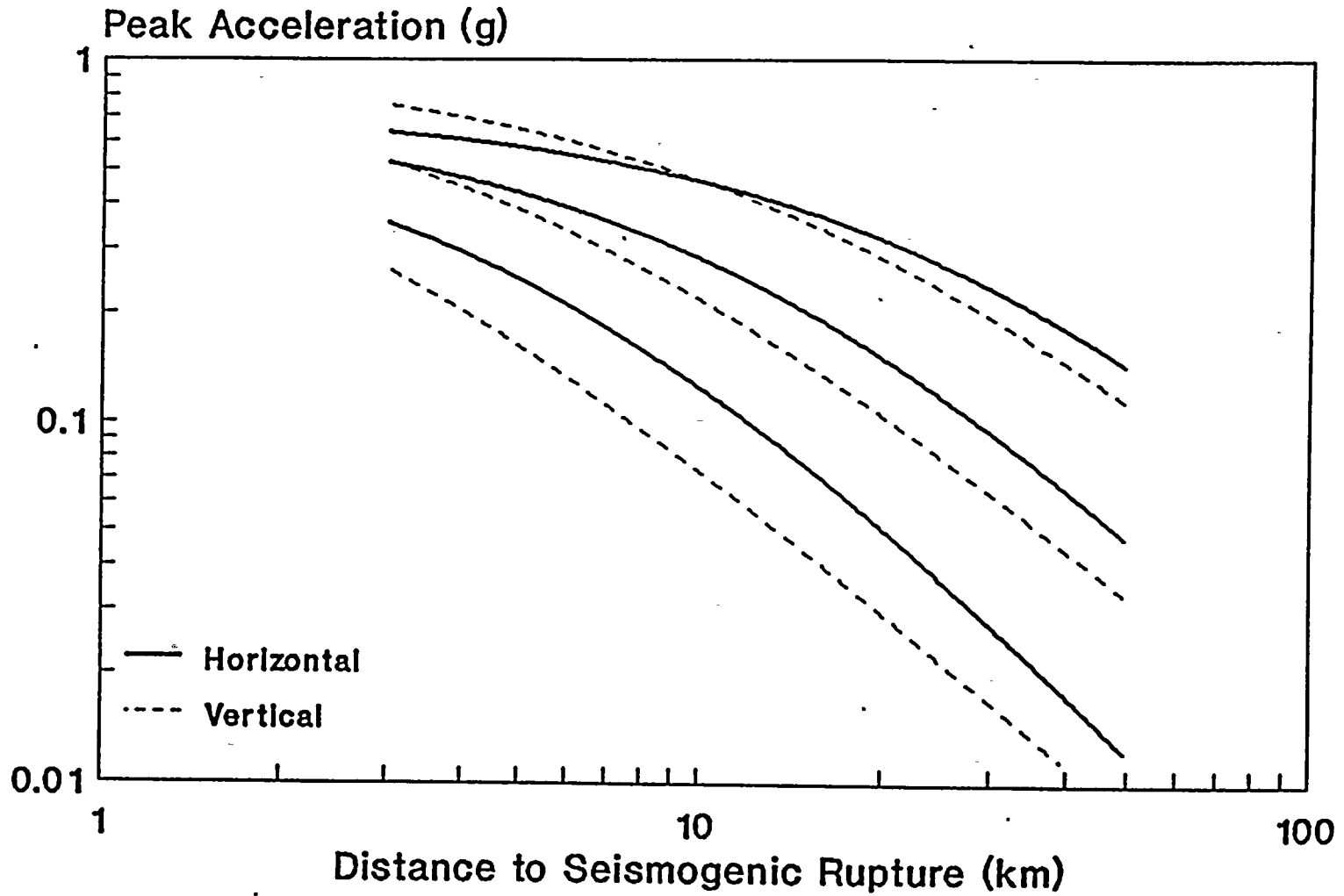


Fig. 5--Attenuation Relationships



# PEAK VELOCITY

Strike-Slip;  $M = 5.0, 6.5, 8.0$ ;  $D = 0$  km

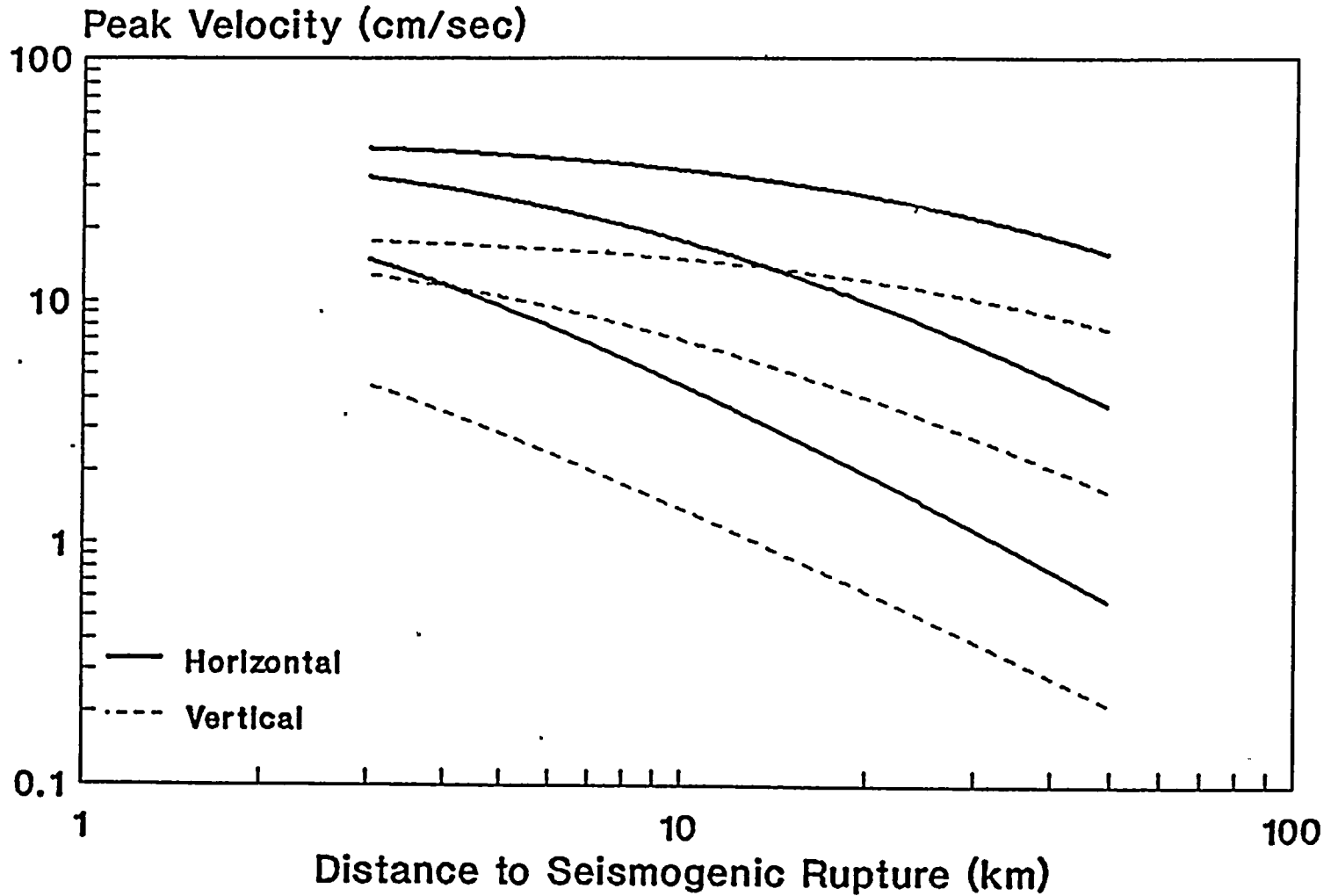


Fig. 6--Attenuation Relationships



**5% DAMPED PSRV SPECTRA**  
Strike-Slip;  $M = 5.0, 6.5, 8.0$   
 $R = 10 \text{ km}; D = 0 \text{ km}$

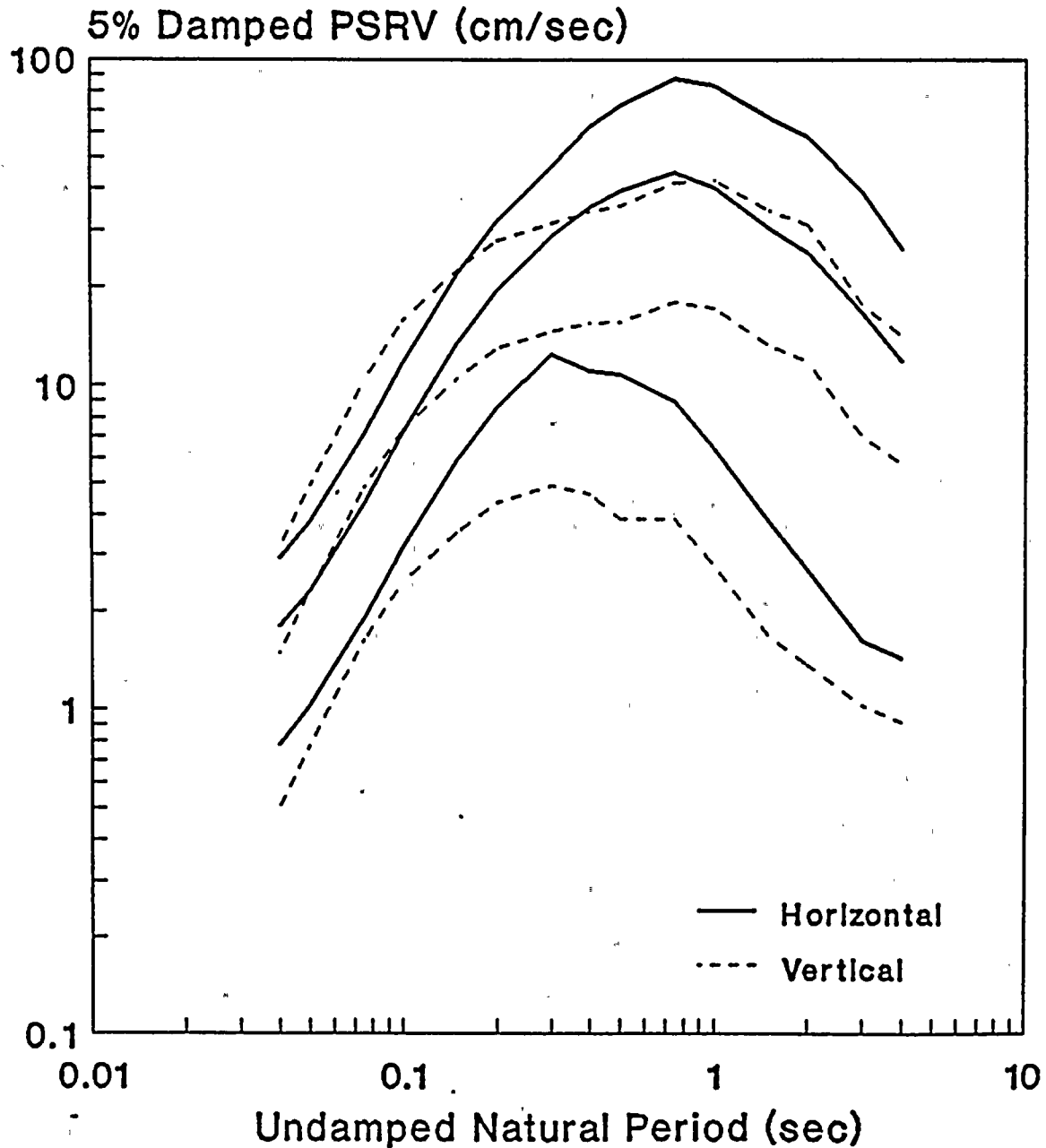


Fig. 7--Pseudorelative velocity spectra



**5% DAMPED PSRV SPECTRA**  
Strike-Slip;  $R = 10, 25, 50$  km  
 $M = 6.5; D = 0$  km

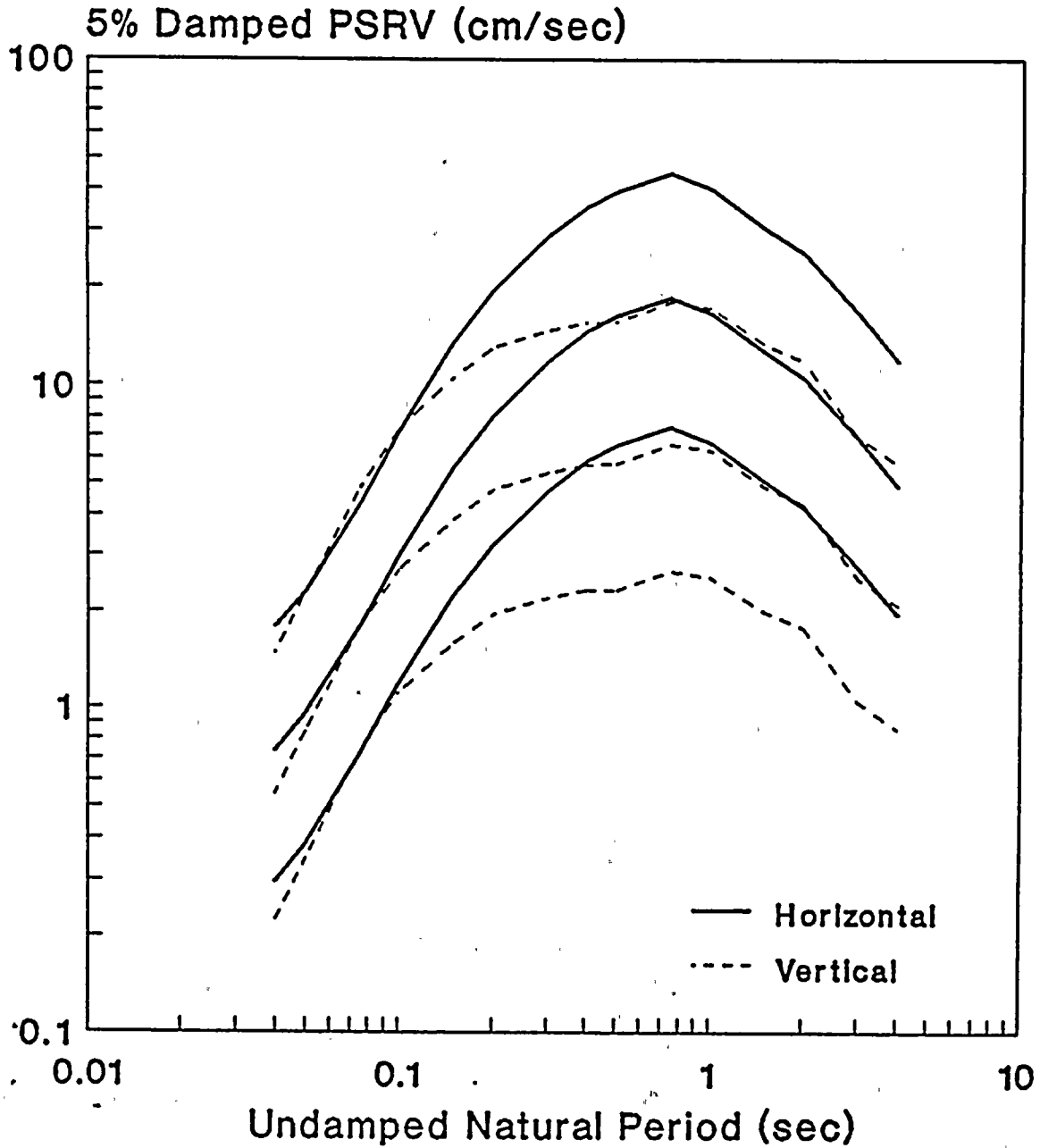


Fig. 8--Pseudorelative velocity spectra



# HORIZONTAL PSAA SPECTRA

Strike-Slip;  $M = 7.2$ ;  $R = 4.9$  km;  
 $D = 4.0$  km

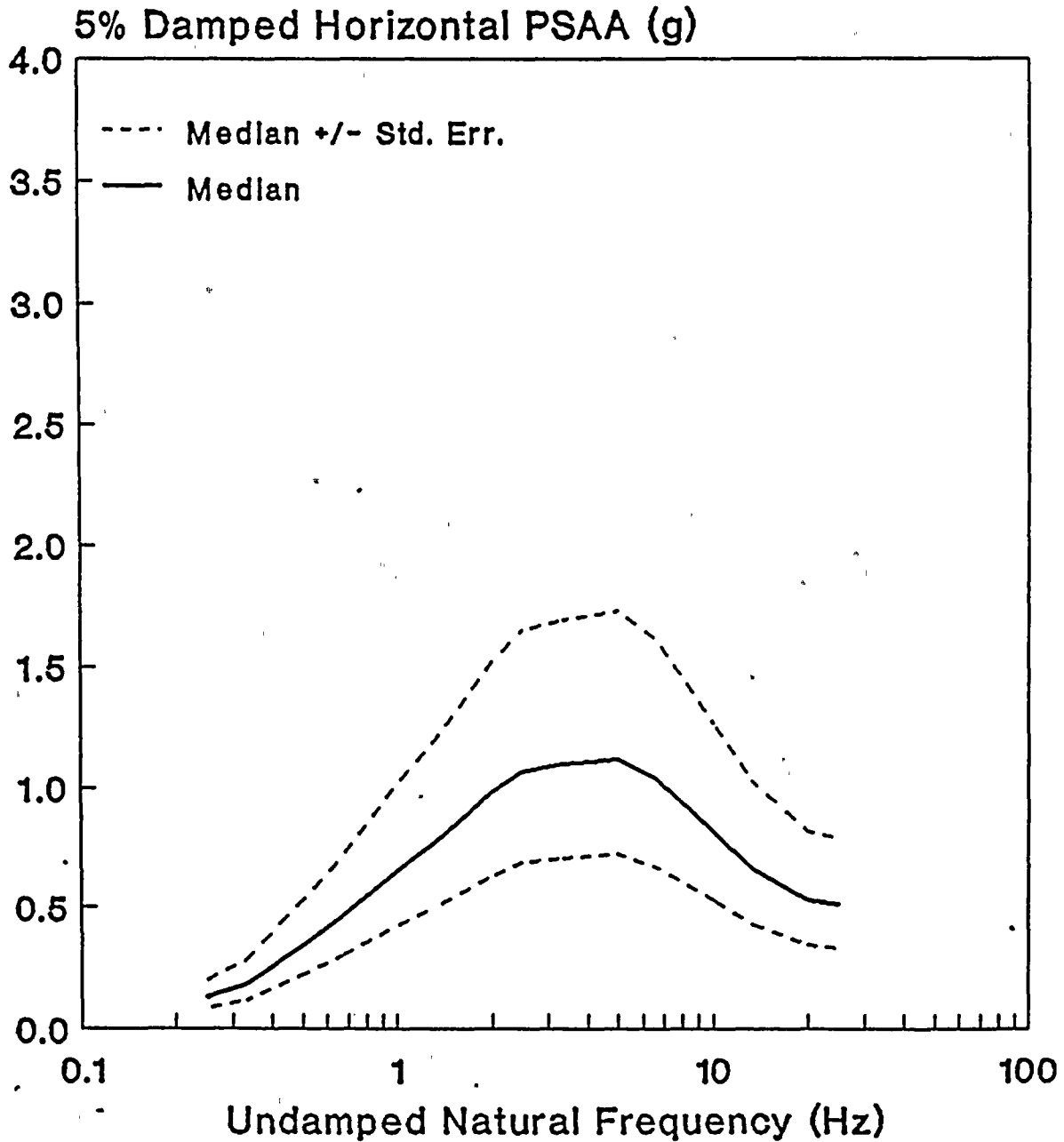


Fig. 9--Predicted LTSP analysis spectra

11  
12  
13  
14



# VERTICAL PSAA SPECTRA

Strike-Slip;  $M = 7.2$ ;  $R = 4.9$  km;  
 $D = 4.0$  km

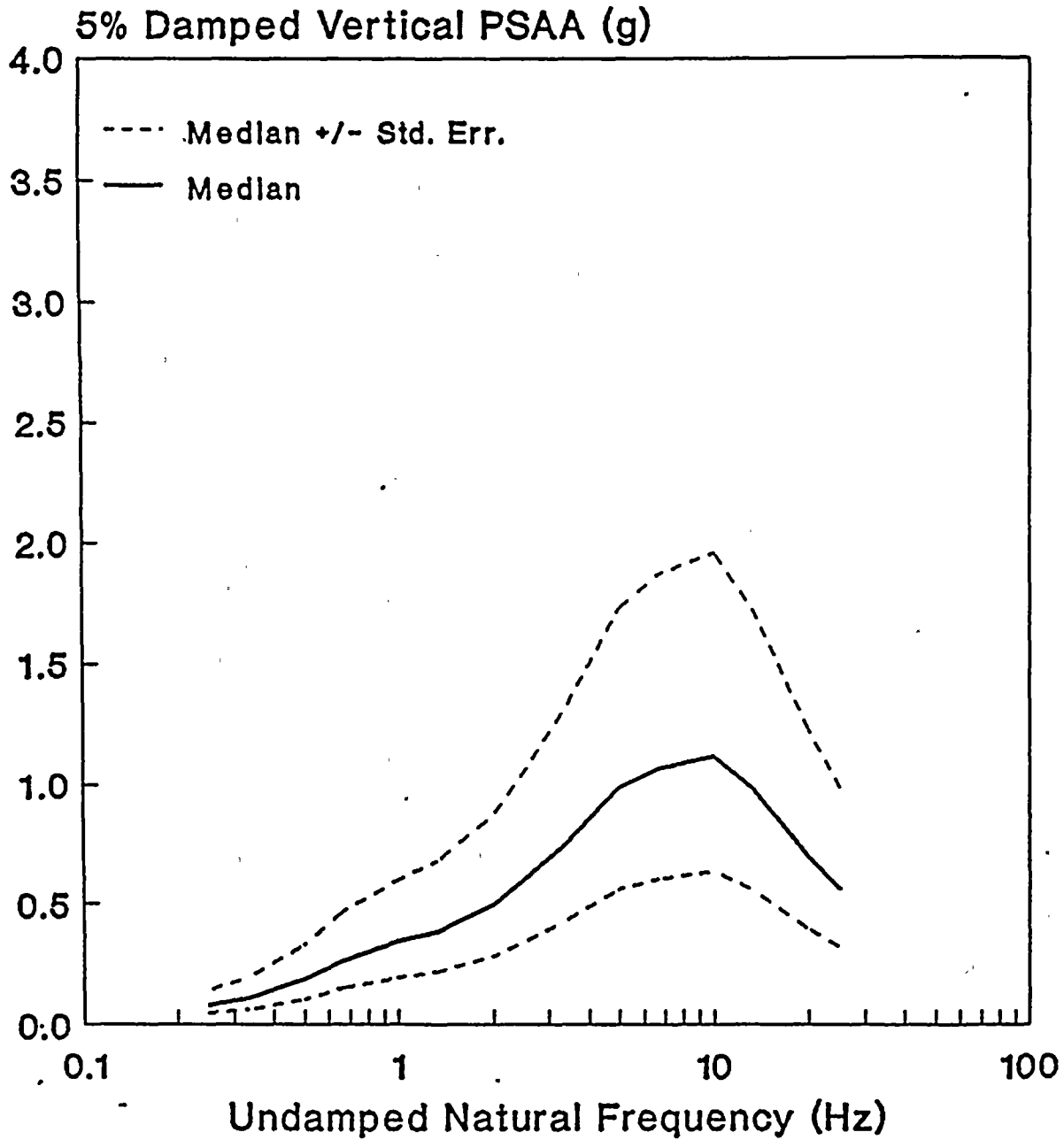


Fig. 10--Predicted LTSP analysis spectra



# HORIZONTAL PSAA SPECTRA

Reverse-Oblique;  $M = 7.2$ ;  $R = 4.7$  km  
 $D = 4.0$  km

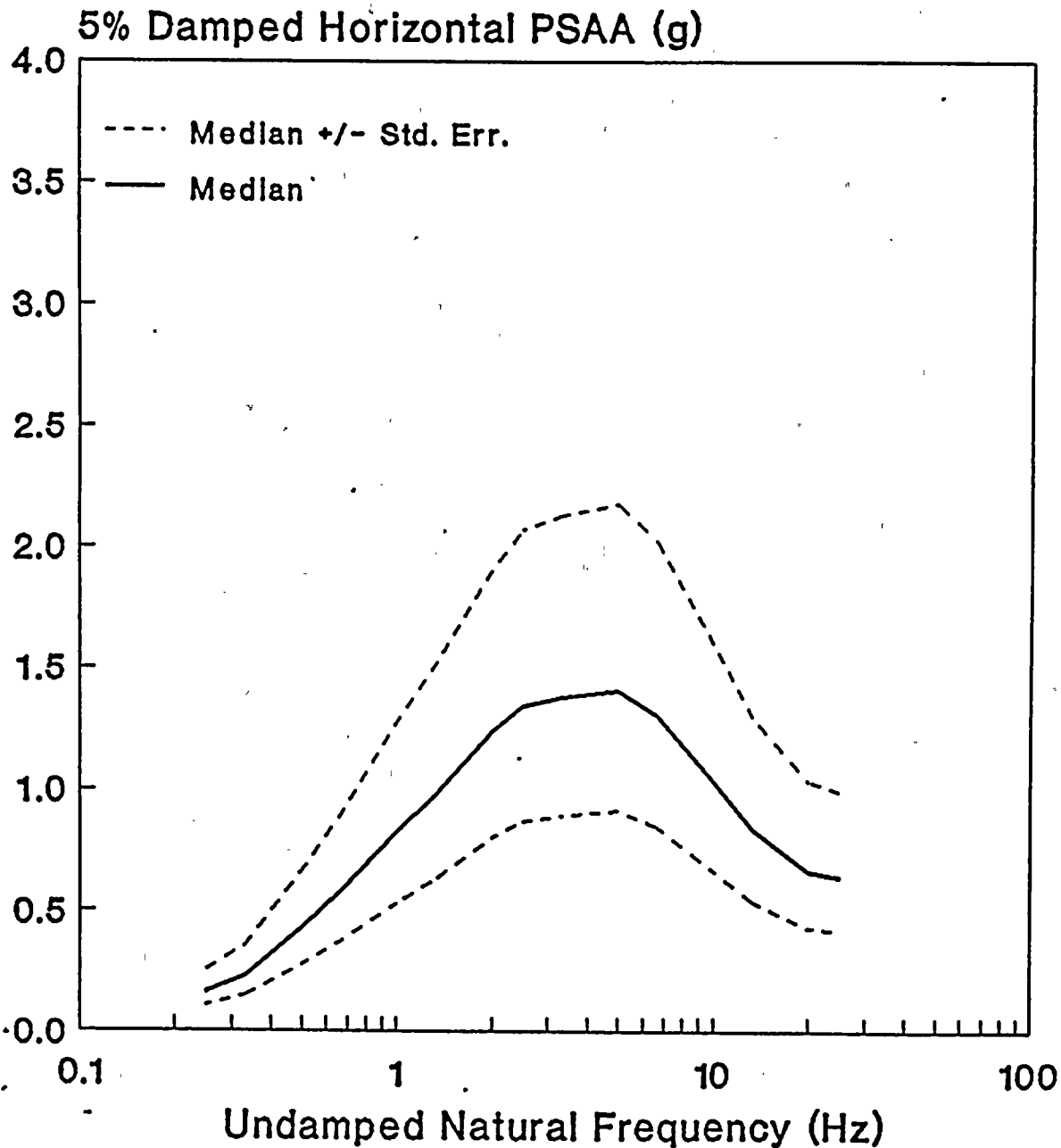


Fig. 11--Predicted LTSP analysis spectra



**VERTICAL PSAA SPECTRA**  
Reverse-Oblique; M = 7.2; R = 4.7 km  
D = 4.0 km

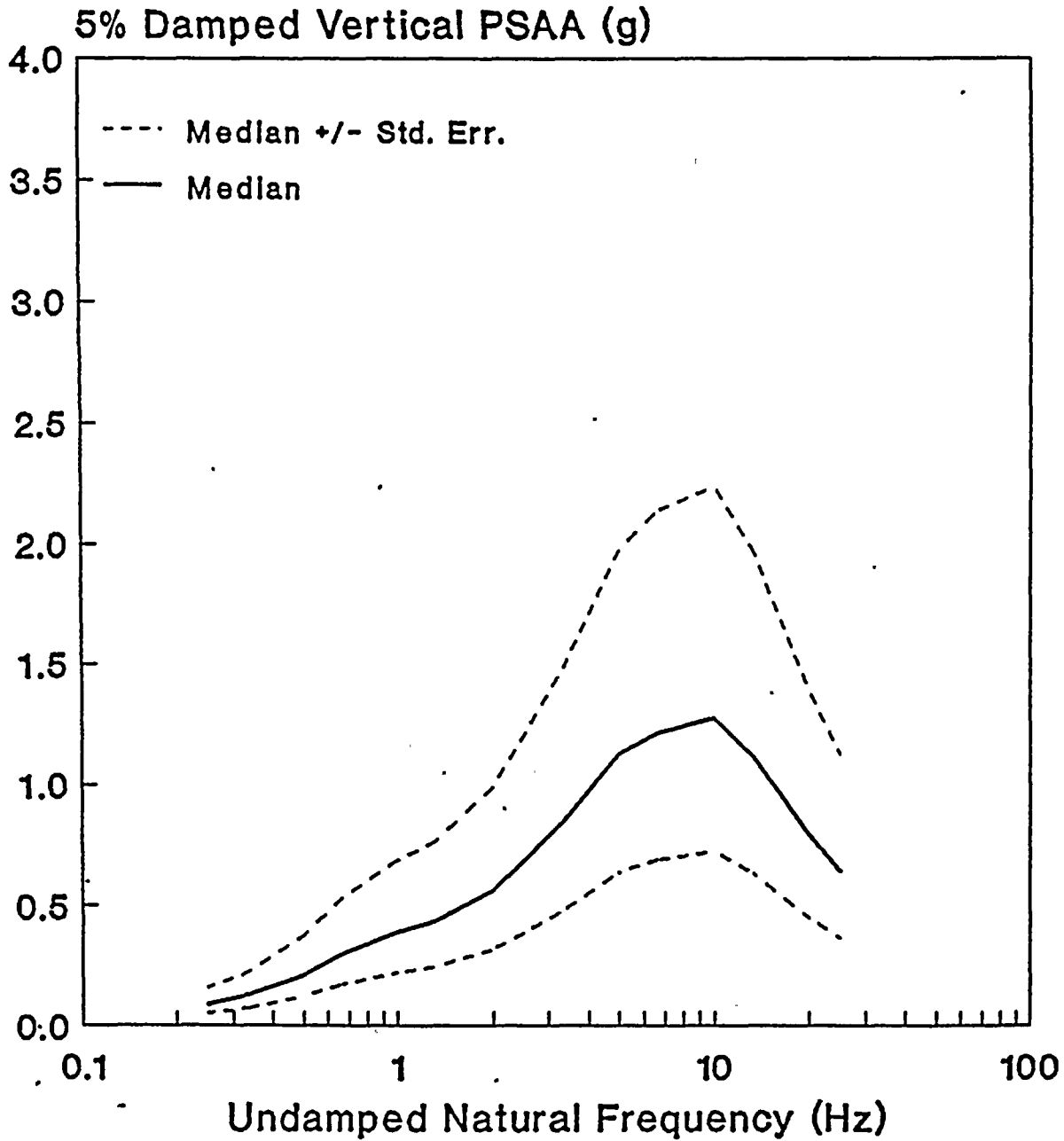


Fig. 12--Predicted LTSP analysis spectra

1 1 1 1 1  
1 1 1 1 1  
1 1 1 1 1  
1 1 1 1 1



# HORIZONTAL PSAA SPECTRA

Thrust;  $M = 7.2$ ;  $R = 5.1$  km

$D = 4.0$  km

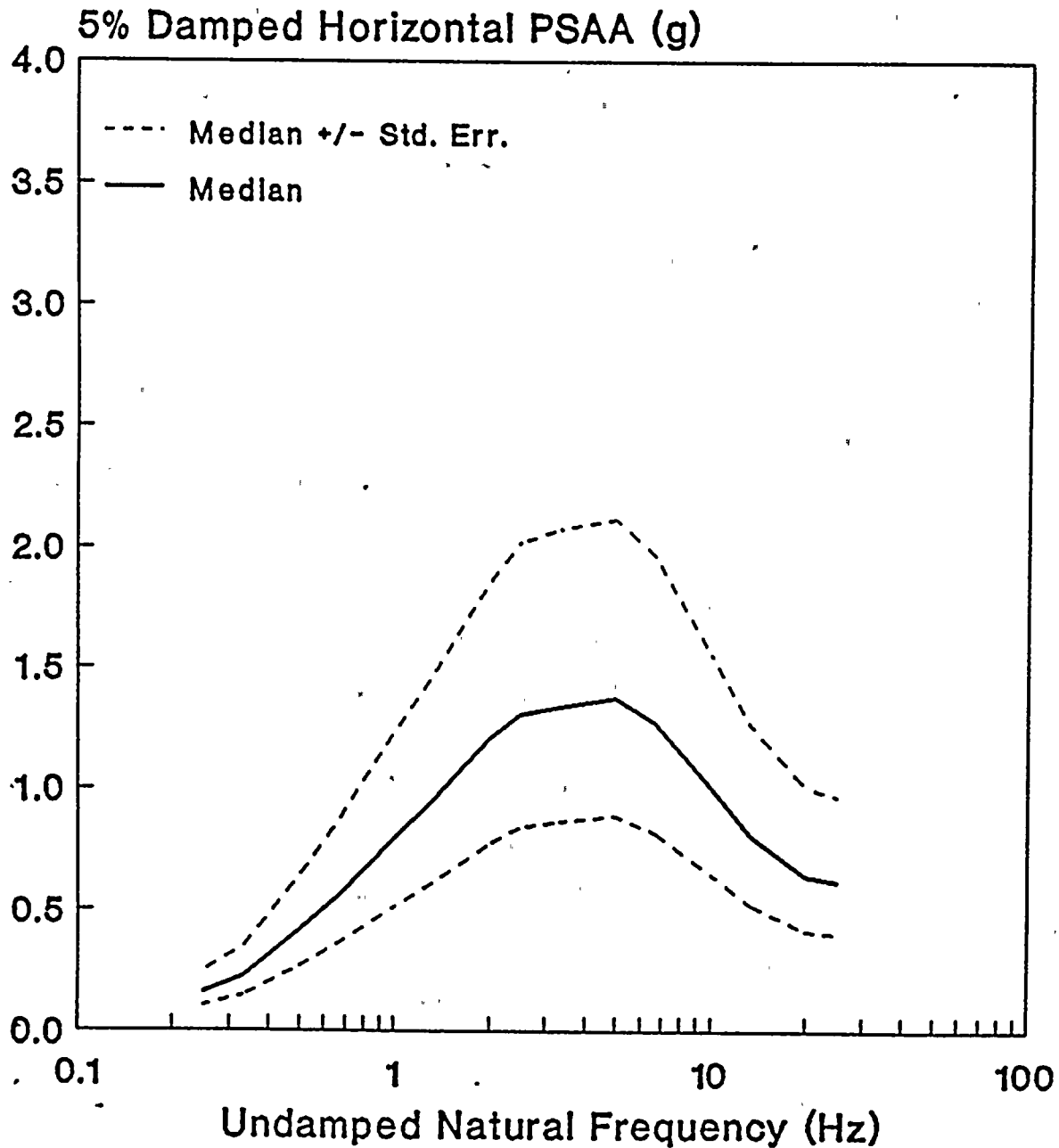


Fig. 13--Predicted LTSP analysis spectra

10  
11  
12  
13  
14



# VERTICAL PSAA SPECTRA

Thrust; M = 7.2; R = 5.1 km

D = 4.0 km

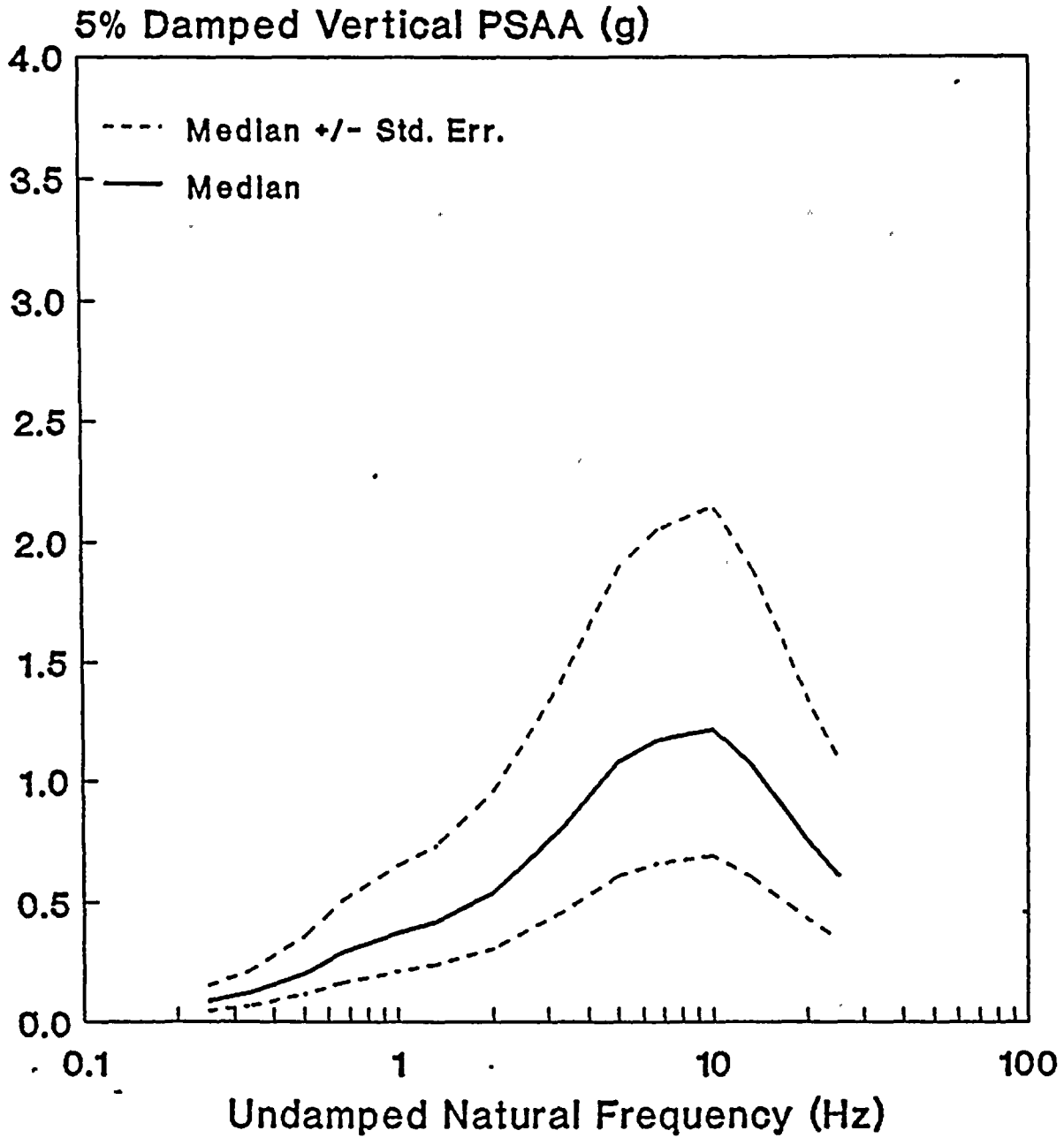


Fig. 14--Predicted LTSP analysis spectra

12/27/77  
12/27/77  
12/27/77  
12/27/77



DATA APPENDIX OMITTED FOR  
TIME BEING — TABLES ARE SIMILAR  
TO THOSE IN USGS OF 89-484

100  
100  
100  
100  
100

